

IN-LINE FIBER OPTIC SENSING SYSTEM FOR PIPELINE CORROSION DETECTION

A Thesis
Submitted to the Graduate Faculty
of the
North Dakota State University
of Agriculture and Applied science

By

Xiao Liang

In Partial Fulfillment of the Requirements
for the Degree of
MASTER OF SCIENCE

Major Department:
Civil and Environmental Engineering

March 2015

Fargo, North Dakota

North Dakota State University

Graduate School

Title

IN-LINE FIBER OPTIC SENSING SYSTEM FOR PIPELINE
CORROSION DETECTION

By

Xiao Liang

The Supervisory Committee certifies that this *disquisition* complies with North Dakota State University's regulations and meets the accepted standards for the degree of

MASTER OF SCIENCE

SUPERVISORY COMMITTEE:

Dr. Ying Huang

Chair

Dr. Fardad Azarmi

Dr. Zhibin Lin

Approved:

04/07/2015

Date

Dr. Dinesh Katti

Signature

ABSTRACT

To understand the impact of corrosion on metal on-shore buried transmission pipeline, which is one of the most critical damages, corrosion evaluation plays an important role. An effective approach for real-time in-line detection of corrosion is still not fully developed yet. This study introduces a concept of using an in-line optical fiber sensor system embedded inside metallic corrosion-resistant coating to conduct corrosion detection.

Fiber Bragg grating sensors were selected as sensing units and the metallic corrosion-resistant coating was achieved using the high velocity oxygen fuel thermal spraying technique. The successful embedment technique was developed by using stainless steel adhesive protection during coating process. Accelerated corrosion tests were performed on four coated steel plate samples with embedded sensors. Both electrochemical and the embedded sensing system were used to assess the corrosion status of the samples. The test results proved the possibility of this method which can potentially apply for metal pipelines.

ACKNOWLEDGMENTS

I would like to express my deepest appreciation to my advisor, Dr. Ying Huang, who had patience and passion for guiding me through this study. Her professional knowledge helped me to overcome many obstacles in this research. I would like to thank my committee member, Dr. Fardad Azarmi, who gave me the best support for laboratory testing for thermal spraying coating which is a new field I was not familiar with before this study. Thanks also go to Dr. Zhibin Lin, who supported me as an advisory committee member.

I also would like to express my appreciation to Dr. Yechun Wang from the Department of Mechanical Engineering, NDSU, who gave me valuable help on electrochemical testing for this study. In addition, a special thank you goes to Fodan Deng, who assist data analysis for corrosion testing results for this study.

Last but not the least, I am grateful to acknowledge and thank all of colleagues who assisted me and to my family for their love and the continuous support in my graduate program at North Dakota State University.

TABLE OF CONTENTS

ABSTRACT.....	iii
ACKNOWLEDGMENTS	iv
LIST OF TABLES	vii
LIST OF FIGURES	viii
1. INTRODUCTION.....	1
1.1. Background	1
1.2. Principles of Corrosion.....	3
1.3. Existing Technologies for Corrosion Detection	4
1.4. Fiber Optic Sensors for Corrosion Detection.....	6
1.5. Coating Techniques for Metallic Pipelines	8
1.6. Objectives and Organization of This Thesis	11
2. FIBER OPTIC SENSOR SELECTION	13
2.1. Operational Principle of The FBG Sensors.....	13
2.2. Corrosion Detection Using FBG Sensors	15
2.3. FBG Sensor Selection	17
2.4. Sensor Calibration.....	18
2.5. Summary	20
3. DEVELOPMENT OF SENSOR EMBEDMENT TECHNIQUE	21
3.1. Securing Bare FBG Sensors with Tapes During the HVOF Process	21
3.2. Attaching FBG Sensors in Place Using Epoxy.....	23
3.3. Protecting Sensors by A Combination of Hypodermic Tube and Epoxy	26
3.4. Securing Embedment Using High-Temperature Resistant Adhesives	28

3.5.	Sample Preparation for Corrosion Tests.....	30
3.6.	Summary	35
4.	ACCELERATED CORROSION TESTS	37
4.1.	Fundamentals of Electrochemical Corrosion Testing Method	37
4.2.	Laboratory Electrochemical Corrosion Tests and Results	39
4.3.	Corrosion Detection Using The Developed In-line FBG Sensors	43
4.4.	Summary	46
5.	CONCLUSION AND FUTURE WORK	48
6.	REFERENCES	50

LIST OF TABLES

<u>Table</u>	<u>Page</u>
1. Center Wavelength Changes of FBG Sensors before and after Coating Process	34
2. Sensors Wavelength Analysis	35
3. Measured Corrosion Rate for Coated Samples from Electrochemical Method.....	43

LIST OF FIGURES

<u>Figure</u>	<u>Page</u>
1. U.S. Pipeline Mileage from 2003 to 2012	1
2. Spray Coating Process Temperature and Particle Velocity [56]	10
3. The HVOF Spraying Process [58]	10
4. FBG Sensor Working Principle [60].....	14
5. (a) Optical Spectrum Analyzer and (b) Typical FBG Spectrum	15
6. Wavelength Change versus the Mass Loss [65].....	16
7. (a) The OS1100 Bare FBG Sensor, (b) The OS3120 Steel Packaged Sensor, and (c) The OS4210 Temperature FBG Sensor	18
8. (a) Sample Used in Calibration Test and (b) SATEC Tensile Machine	18
9. (a) Calibration Test Results at Loading Rate of 62.2 N/s and (b) Loading Rate of 17.8 N/s	19
10. Temperature Calibration Test Results	20
11. Thermal Spraying Robotic Arm and Test Set-up for the First Embedment Test	22
12. (a) Recorded Strain Sensor Data and (b) Temperature Sensor Data in First Test.....	23
13. (a) Sensor Attached on a Steel Plate Using M-Bond 200 and (b) Sensor Embedment Test Set-up	24
14. (a) Recorded Strain Sensor Data and (b) Temperature Sensor Data in Second Test ...	25
15. Damaged Area of the OS3120 FBG Sensor after the Second Trail	25
16. (a) Prefabricated Grooves on the Substrate and (b) Sensor Condition after Coating ..	27
17. Samples with (a) Minco Epoxy, (b) Nickel Based Adhesive, and (c) Stainless-Steel Based Adhesive	29
18. Samples with (a) Minco Epoxy, (b) Nickel Based Adhesive, (c) Stainless-Steel Based Adhesive after Sandblasting.....	29

19. Samples with (a) Minco Epoxy, (b) Stainless-Steel Based Adhesive after Thermal Spray Coating process, and (c) Optical Micrograph of the Copper Coating	30
20. (a) Steel Plate Sample and (b) 6 Samples for Testing.....	31
21. Sensor Location of Sample (a) #1, (b) #2, (c) #3, and (d) # 4	32
22. Sandblasted Samples.....	32
23. FBG Center Wavelength Changes during Coating Process for Sample (a) #2, (b) #3, (c) #4 Strain, (d) #4 Temperature.....	33
24. Thermal Spraying Coated Samples.....	34
25. Electrochemical Reaction Principle.....	38
26. Accelerated Corrosion Test Set-up	39
27. Glued Tube on the Sample Surface.....	40
28. (a) Reference Electrode and (b) Accelerated Corrosion Test Set-up	41
29. Tafel Test Result for Sample (a) #1, (b) #2, (c) #3, and (d) #4	42
30. Corrosion visual inspection for Sample (a) #1, (b) #2, (c) #3, and (d) #4	44
31. Center Wavelength Change from the FBG Sensors from the Accelerated Corrosion Test for 21 days.....	46

1. INTRODUCTION

1.1. Background

Using pipelines is the most economical method that exists to transport a large quantity of fluid or liquid, especially petroleum, natural gas, and biofuel. In United States, almost 350 thousand miles of pipelines are underground to power the US economy. Since the first crude oil pipeline was built in the late 19th century, pipeline transportation of petroleum and natural gas has grown rapidly. The oil and natural gas pipeline industry had an annual growth of revenue rate of 1.5% from 2009 to 2014, and a conservative annual growth rate of 1.4% from 2014 to 2019 is predicted [1]. Smith reported [2], the mileage of oil and gas pipeline constructed from 2003 to 2012 had a slightly increase as shown in Figure 1.

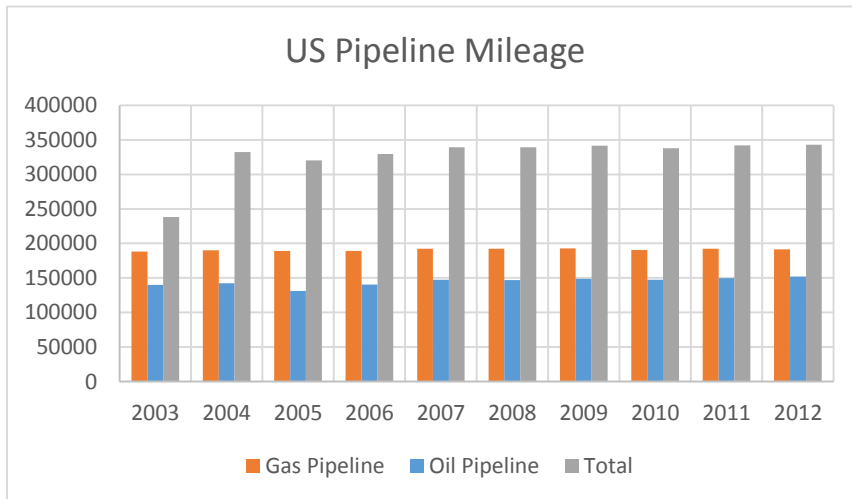


Figure 1. U.S. Pipeline Mileage from 2003 to 2012

In addition, natural gas consumptions continue increasing worldwide due to the economic and environmental considerations. Tubb [3] indicated approximately 75% of total global planned

pipeline will be designed for natural gas. More pipeline mileage internationally is predicted in next decade under the supply and demand phase.

The safety and durability of the pipelines have been brought into public attention since the increasing pipelines mileages and potential large new pipeline construction projects such as the keystone pipeline project. Among various pipeline damages, prolonged pipeline corrosion is one leading reason for failure of on-shore buried pipeline [4, 5] since corrosion may lead to a reduction in structural integrity. In particular, the external corrosion represents 80% of all corrosion induced pipeline accidents [6].

Corrosion could also decay the reliability and durability of pipelines significantly, resulting in the reduction of the pipe's structural performance efficiency and the increase of the maintenance costs and downtime [7]. According to the investigation of U.S. Department of Transportation (U.S. DOT), the on-shore pipeline corrosion related failure and corrosion management expense was around \$7 billion in 2002 [8]. Due to the explosive increase of pipeline industry in recent years, the corrosion related maintenance cost has increased as well. The corrosion cost was above \$1 trillion in 2012, accounting for about 6.2% of GDP. This cost includes the management, monitoring, repair, replacement, and direct and indirect cost of corrosion [9]. In addition, the spillover of hazardous material from corroded or damaged transmission pipelines can have a serious environmental impact and lead to potential fire accidents and human fatalities [10].

Timely pipeline corrosion detection and assessment will significantly help to reduce the increasing costs for corrosion associated maintenance and repair. Various corrosion detection

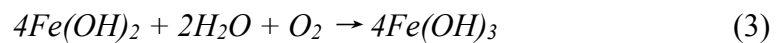
methods were developed for achieving the goal of a timely corrosion assessment. This chapter reviews the fundamental principles of corrosion, the existing corrosion detection technologies available, the fiber optic corrosion sensors developed in recent years, and the protective coating technique used for pipeline corrosion mitigation. Accordingly, potentials for new technologies for effective pipeline corrosion detection are also discussed.

1.2. Principles of Corrosion

Generally, corrosion is an electrochemical process which involves the exchanges of electrons when metal transmission pipeline is exposed to surrounding environment with moisture. Water and oxygen play dominant roles in a corrosion process as time passes [11]. For steel pipes which are the most popular material in pipeline industry, the presence of water and oxygen oxidized the iron to be ferrous ions through the chemical reaction described below:



Further oxidation of Fe^{2+} to Fe^{3+} happens with significant amounts of water and oxygen [12] following the chemical reaction below:



There are many types of corrosions in pipelines, which can be summarized in two categories by the measure of corroded length and width: general and local corrosion. Corrosion can also be analyzed by different corrosion causes, including galvanic corrosion, microbiologically induced corrosion, AC corrosion, and cracking by different soil [13]. The occurrence of external

corrosion on pipelines is a very complicated process. It could be induced by the local environmental factors, such as the pH value changes of soil, local temperature concentration, and the humidity changes. Chemical corrosion can also be accompanied due to the various chemical properties of soil with buried pipeline and the chemical reaction when the surface pipeline is exposed to air. The pipelines also experience adverse effects physically. Human activities and external earth forces from surrounding environment occasionally or persistently impact pipeline's outer surface, especially on buried pipeline with high probability of being constrained with soil pressure and hydraulic pressure. If local damages induced to the pipes, corrosion may happen at these stress concentrated locations. There are many uncountable uncertainties that may lead to the metallic transmission pipeline corrosion as well. For instance, an incorrect operation, such as a welding defect, could accelerate the corrosion process and induce pipeline integrity threat [14]. In this case, eliminating and inspecting pipeline corrosion is a feasible idea to extend pipeline's reliable life-span.

1.3. Existing Technologies for Corrosion Detection

There are two major corrosion assessment approaches including risk based inspection (RBI) and corrosion inspection. The RBI is not currently widely used since this technique has an impediment in that it must be worked with corrosion risk assessment or other risk analysis to make a unique physical inspection process plan. Another limitation of RBI is that it only focuses on the most critical area of a structure [15] and it is not efficient for large scale structures as to pipelines.

Corrosion inspection is a very powerful and impactful inspection technique [16]. For corrosion inspection, there are three types of inspection approaches including the material sacrificial, electrochemical, and physical methods. The material sacrificial is the earlier technique that can measure the direct corrosion-induced mass loss of materials [17]. It is a simple technique, requiring a destructive approach to measure the metal loss by gravimetric methods while the oxidized corrosion product had been removed [18]. The destructive nature of this technique induced safety concerns of pipes. Even though the removal of a small piece from a pipe is feasible, it may affect the structural integrity. In addition, the small testing piece from the main body may not represent the corrosion condition of the entire structure. To avoid a destructive testing, as an alternative, material coupons can be placed on the side of the assessing pipes for the metal loss measurement purpose. Thus, the material sacrificial technique can only have corrosion measured by the scheduled detection periodically and the operation of the testing is very time-consuming since corrosion is a long-term process, even it remains a reliable reference method [19].

The electrochemical technique can be applied since this is a non-destructive measurement of pipeline corrosion. The electrochemical technique is currently the most widely used approach for corrosion measurement. This method measures the electric field or potential differences on corroded steel surface to acquire the electrochemical corrosion related details [20]. It can measure corrosion types and corrosion rates with parameters by using various instruments, hardware, and software to perform various analysis routines as well [21]. However, electrochemical approach measures the average corrosion rate of an object, and it measures the impedance of a relatively

large area. Also, the electrochemical technique is not a remote approach that requires experienced technicians on site for testing.

Physical approaches may also be considered for corrosion detection if direct electrochemical measurement is not possible. The physical method for corrosion measurement acquires corrosion related parameters, such as the environmental pH value changes, temperature variation, and the electrical conductivity changes. These parameters can be correlated to the corrosion behavior of the metal pipes by statistical calibration. By evaluation those parameters and metal behavior, the corrosion magnitude and corrosion rate could be estimated [22, 23]. However, this method also requires experienced technicians or trained specialists for testing.

From the above review, it can be seen that to date a remote and online corrosion detection which is essential to monitor the corrosion of pipes is not yet developed. Fiber optic sensors is potentially a tool for providing a remote and online corrosion measurement for pipelines, due to their unique advantages of being compact in size, environmental durable, electrically charge free, highly sensitive, variable in form, able to multiplexing, and immune to electromagnetic interference [12, 20, 24-26].

1.4. Fiber Optic Sensors for Corrosion Detection

The Fiber optic based sensing technique provided a remarkable progress and accuracy level in structural health monitoring of civil engineering field [27]. It has been widely used for the measurements of strain [28] and vibrations [29] etc in civil engineering applications. Based on the

measurement principle, several types of fiber optic sensors have been investigated for corrosion detection, including intensity or interferometer based and grating based sensors.

To detect potential corrosion, the interferometer-based optical fiber sensors monitor the light intensity changes induced by the coating thickness changes on the cleaved fiber end or an uncladded portion if a thin-film metal layer is coated and corroded away. The investigated metals for this purpose included Fe–C alloy [30], iron [31], Ni–P and aluminum [32, 33], nickel, and silver [34]. The concept for the intensity or interferometer-based fiber optic sensor is simple and easy to operate. However, multiplexing large amounts of these sensors becomes a challenge and results in a high cost for the corrosion monitoring for large-scale structure, such as pipelines.

Fiber grating sensors attract a worldwide attention for a more cost effective approach. Two types of fiber grating sensors exist including the long period fiber grating (LPFG) and fiber Bragg grating (FBG). The LPFG sensors have been applied to monitor corrosion environments for aging aircrafts [35] that can be indirectly related to the corrosion process such as moisture, pH, and metal ion. In addition, the LPFG sensors also were developed to directly measure corrosion process for steel structures [36, 37]. The LPFG sensors are very sensitivity to the environments, thus, to the corrosion. However, since the LPFG sensors are sensitive to various other environmental factors, the direct correlation between the detected wavelength changes with the corrosion is hard to establish.

On the other hand, the FBG sensors, which are not sensitive to the environmental factors other than temperatures, have been studied as physical based corrosion sensors. The FBG sensors

measured corrosion-induced strains which can be related to the corresponding corrosion condition [38]. Wrapping technique [38], thin metal coatings on top of the sensing unit [39], or pre-strained technique [40] were investigated to induce the strain changes corresponding to the corrosion. The FBG sensors are very reliable and cost-effective. However, same as the LPFG sensors, the FBG sensors, which are made by glass fiber with a negligible diameter, is very fragile in their bare form and subject to breakage when being handled improperly when transporting, installing, and maintaining [41].

To improve the reliability of the FBG sensors, various sensor packaging methods had been designed for different purpose with more applications of the FBG sensors in civil engineering fields. Flexible polyvinyl chloride (PVC) skin foil was used to protect the fiber sensors from harsh environments or exposing to chemical condition [42]. Epoxy resin had been investigated [43] for protecting the sensors from external forces. Carbon or glass fiber reinforced polymer was also applied as packaging materials for fiber optic sensors' applications in structure [44], roadway [45], pipeline [46] crack or deformation detection, and corrosion detection [38]. However, these packaging methods, which mostly were developed for the purpose of using the fiber optic sensors for structures' mechanical behavior sensing, is not applicable for corrosion detection of pipelines, resulting in needs for the development new packaging methods.

1.5. Coating Techniques for Metallic Pipelines

Coating technologies had been widely applied to prevent or mitigate pipeline corrosion. Two categories of coatings are existing for the mitigation of pipe corrosion: the nonmetallic (soft)

and metallic (hard) coatings. The non-metallic coatings separate the metal pipeline from the surrounding corrosive environments, showing a good performance on corrosion mitigation. Coal tar coatings [47] were designed and applied to pipeline before 1970s, which were difficult to apply and environmentally unfriendly. For a safer, faster, stronger, and easier coating, solid rigid polyurethane coating [48] were developed for pipeline corrosion prevention in 1970s and replaced the coal tar based coating in 1980s. Since, thin solid rigid polyurethane coatings may fail corrosion protection after long-term uses, thick layered coatings were developed in 1990s including polychloroprene coating [49], Fusion-Bonded Epoxy- (FBE) coating [50] and 3-Layer-Polyurethane coating (3LPE) [51]. Combined with concrete, the FBE or 3LPE coatings were widely deployed in off-shore pipelines. These thick polymer coatings have disadvantages such as high cost and high potential for initial defects. Thus, the organic substances, such as polyimide, polyurethane, or conductive polymer [52], ceramic, epoxy, and resin become popular as non-metal coating materials recently. So the hard metallic coating had been considered for corrosion protection.

Hard metallic coatings can also be used for corrosion protection [53] and one technique called thermal spraying technique has been used to protect the steel production from corrosion since the 1970s [7]. The thermal spray coating technique attaches molten material, semi-molten material, or powder onto almost any object by spraying to build up a thin layer of hard coating [54]. The heat to melt the material or powder can be provided by the high velocity oxygen fuel

(HVOF), radio frequency (RF) plasma, or direct current (DC) plasma [55] as seen in Figure 2, which can be categorized by particle velocity and process temperature.

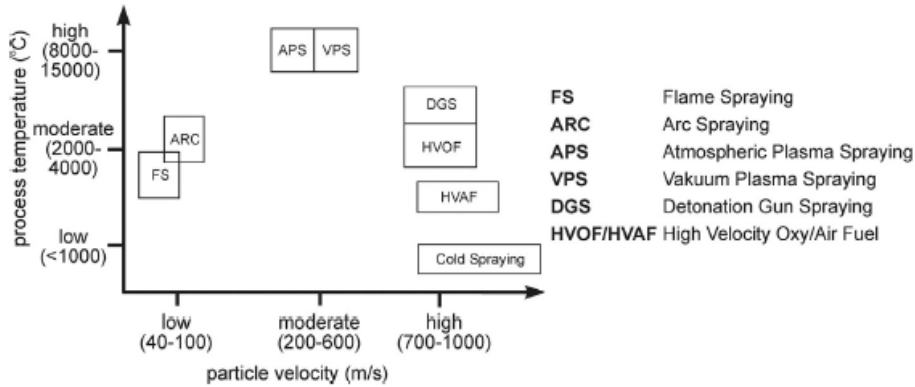


Figure 2. Spray Coating Process Temperature and Particle Velocity [56]

Among all the thermal spraying techniques, the HVOF spray technique used widely [57]. The HVOF thermal spraying technique uses a spray gun that applies a combustion condition that mixes the oxygen and fuel to generate a gas stream with ultrasonic velocity as shown in Figure 3. Since the molten metal or powder is transported into combustion chamber of spray gun, the molten metal or powder particles are accelerated and combine with gas stream spray onto the surface of substrate via a converging-diverging nozzle. The splat impact each layer and form coating by the mechanical bonding [54].

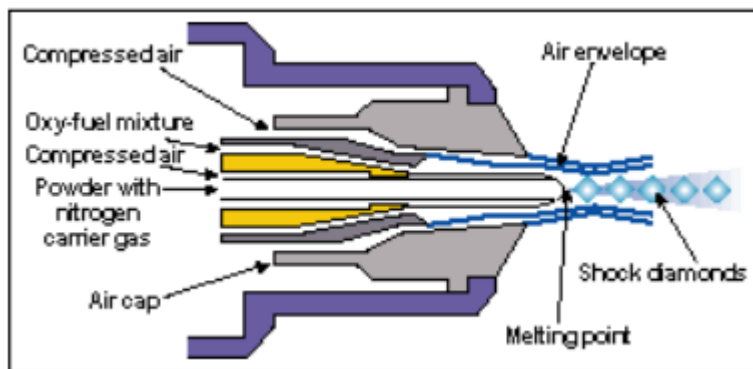


Figure 3. The HVOF Spraying Process [58]

1.6. Objectives and Organization of This Thesis

In this study, an innovative in-line fiber optic sensor system will be developed through packaging the sensors by metallic hard coatings using the HVOF thermal spraying technique to detect the pipeline corrosion remotely in an online manner and at the same time mitigate the pipelines from corrosion. The fiber optic sensors will be embedded inside the HVOF thermal sprayed hard coating with a thickness in range of 50-500 μm . With the integrated system, the metallic pipelines will be protected from corrosion and meanwhile monitored for their corrosion status. Thus, the specific objectives of this thesis include:

- 1) The selection of appropriate fiber optic sensors for the purpose to detect corrosion status when embedded inside a HVOF sprayed hard metallic coating;
- 2) The development of sensor embedment technique which could survive the harsh environments during the HVOF thermal spraying process;
- 3) The validation of the developed fiber optic sensor based corrosion detection system through laboratory accelerated corrosion tests.

To achieve the objectives mentioned above, this thesis is organized as follows: In Chapter 1, an introduction of pipeline corrosion and a detail literature review are performed; In Chapter 2, the fiber optic sensor is selected based on the application requirements and the corrosion detection principles are analyzed using the selected sensors; Chapter 3 details the challenge-solving of the development of sensor embedment technique using the thermal spraying coating; Chapter 4 discusses the laboratory accelerated corrosion tests performed on the sensor samples and the test

results; and in Chapter 5, conclusion and future work has been presented based on the findings from this study.

2. FIBER OPTIC SENSOR SELECTION

Fiber Bragg grating (FBG) sensor has been selected to be embedded inside the hard metallic coatings in this study to form a physical based corrosion sensing system for pipeline corrosion detection. Fiber Bragg grating sensor has its unique advantages when compared with other optic sensors, such as good reliability and repeatability, no interference from surrounding environments, low cost, and capacity of multiplexing large amount of sensors in a single fiber [27]. In this chapter, the operational principle of the FBG sensor, potential corrosion detection concept using FBG sensors, the specific selections of temperature and strain FBG sensors, and their sensor calibration, are introduced in detail.

2.1. Operational Principle of The FBG Sensors

Fiber Bragg grating sensor produces a periodic modulation with effective refractive index in the core of photosensitive optical fiber [59]. With light transmitted through the grating, a Bragg wavelength (λ_B) will be formulated by the reflection of the light signal periodically, which is defined as the Bragg condition. The Bragg wavelength can be determined by the effective refractive index (n_{eff}) of the optical fiber and the grating period (periodic spacing of grating) (Λ) [12, 28] as follows:

$$\lambda_B = 2n_{eff} \cdot \Lambda \quad (4)$$

Corresponding to the change of external strains or temperatures, the grating period, Λ , will be changed proportionally, resulting in a shift with Bragg wavelength as shown in Figure 4. The magnitude of this shift can be calculated as [12, 28]:

$$\Delta \lambda_B / \lambda_B = (1 - P_e) \cdot \varepsilon + \zeta \cdot \Delta T \quad (5)$$

where, the P_e represents the photo-elastic constant of a fiber, which is related to the fiber property, ε is the strain on the fiber, ξ is a thermo-optic coefficient constant based on fiber property, and ΔT represents the temperature variation.

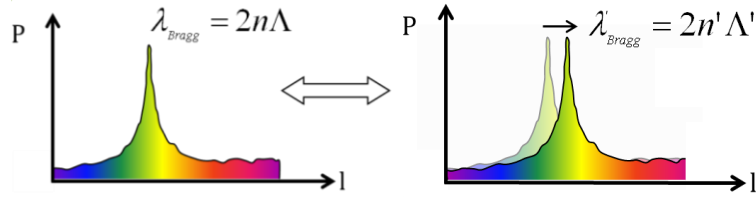


Figure 4. FBG Sensor Working Principle [60]

If a FBG temperature sensor (with initial center wavelength of λ_T) is available for compensation and measures the temperature induced center wavelength changes of $\Delta\lambda_T$, the strain on the fiber due to the physical behaviors can be obtained as [12, 28]:

$$\varepsilon = \frac{1}{(1 - P_e)} \left(\frac{\Delta\lambda_1}{\lambda_1} - \frac{\Delta\lambda_T}{\lambda_T} \right) \quad (6)$$

Thus, by embedding a FBG strain sensor and a temperature reference sensor inside a hard coating on a pipeline, the sensors are able to detect the strain variance induced inside the coating continuously. If the strain variance is induced by the corrosion, then the corrosion status can be evaluated correspondingly, which forming a physical corrosion detection technique for metallic pipelines remotely and in line.

In this study, a National Instruments NI PXIe-1017 optical spectrum analyzer was used as shown in Figure 5(a) for the instrument to record the Bragg wavelength changes of the FBG sensors continuously and 5(b) for a typical FBG spectrum.

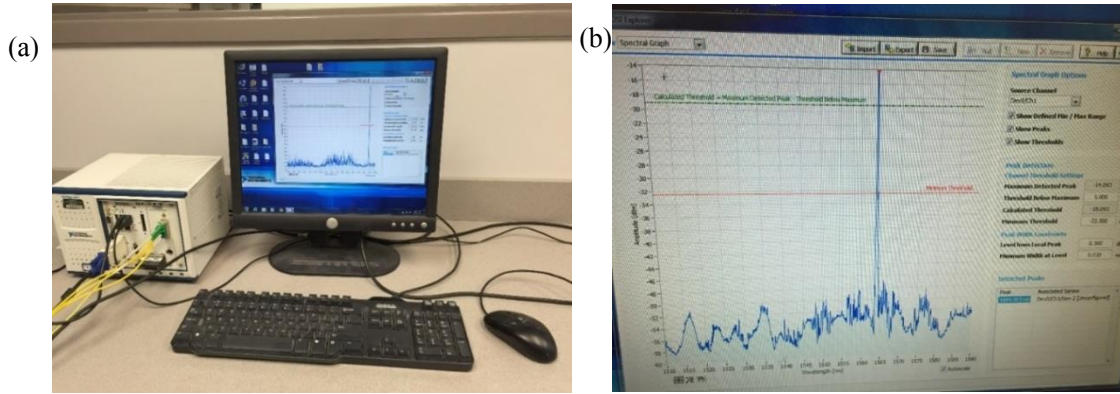


Figure 5. (a) Optical Spectrum Analyzer and (b) Typical FBG Spectrum

2.2. Corrosion Detection Using FBG Sensors

FBG sensors had been investigated for corrosion detection on various reinforced concrete and steel structures [61, 62]. Based on Eq. (6), by measuring FBG center wavelength changes from corrosion induced strain changes, two major hypotheses had been studied: 1) the corrosion induces strain changes from the volume expansion through the corrosion rust production process, and 2) the corrosion process releases strains prefabricated on FBG sensors.

Using the concept of volume expansion inducing strain changes, several researchers [63, 64] aligned the FBG sensors in the circumferential direction on steel reinforcements to monitor the corrosion in RC structures. The corrosion rate, ρ , thus, could be obtained using the rate of circumferential volume expansion from the corrosion as follows [63]:

$$\rho = \frac{\Delta V}{V_0} = \frac{(D_0 + \Delta D)^2 - D_0^2}{D_0^2} = \left(1 + \frac{\Delta D}{D_0}\right)^2 - 1 = (1 + \varepsilon)^2 - 1 \quad (7)$$

in which ΔV is the volume changes, V_0 is the original volume of the steel reinforcement, D_0 is original diameter of steel rebar, ΔD is diameter change through corrosion process, and ε is the strain changes induced in the corrosion process.

Combining Eqs. (6) and (7), the corrosion rate of the steel reinforcements can be obtained using the monitored wavelength changes ($\Delta\lambda$) as below:

$$\rho = \left(1 + \frac{\Delta\lambda}{1-P_c}\right)^2 - 1 \quad (8)$$

Pre-strained FBG sensors also had been investigated for corrosion detection [40, 65] based on the hypothesis that the mass loss during the corrosion process would cause the prefabricated strains on the FBG sensors to gradually relax till the release of all the pre-strains. The pre-strain loss induced center wavelength shifts during the corrosion process could be monitored with the immersion time. With periodic measurement of corrosion induced mass loss, the relation between the mass loss and the center wavelength changes can be obtained using Eq. (9) according to measurement results as shown in Figure 6 [65]:

$$\frac{\Delta M}{S} = -3.13 \times 10^{-4} \ln\left(\frac{248.64}{\Delta\lambda + 249.91}\right) \quad (9)$$

where, $\frac{\Delta M}{S}$ is the mass loss per unit surface area.

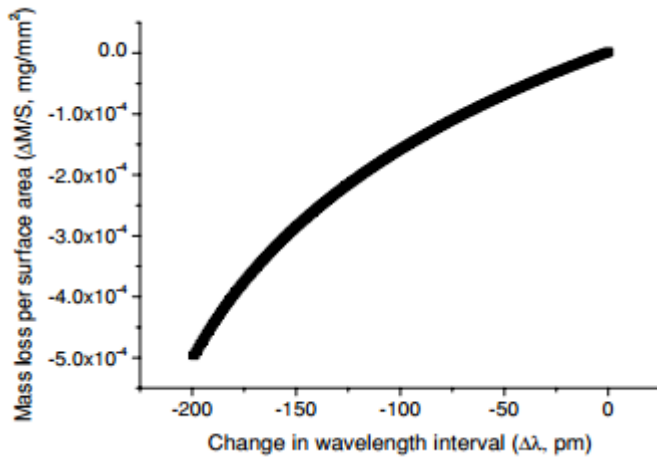


Figure 6. Wavelength Change versus the Mass Loss [65]

In this study, both hypotheses will be considered for the corrosion detection with embedded FBG sensors inside the HVOF coating. The hypothesis which fits the detection results the most will be further studied numerically in future.

2.3. FBG Sensor Selection

Three types of FBG sensors from Micron Optics Company were selected in this study, including two strain sensors and one temperature sensor. The first strain sensor is the OS1100 FBG sensor as shown in Figure 7(a), which is a bare FBG sensor coated with polyamide. It has a strain sensitivity of $1.2 \text{ pm}/\mu\epsilon$, a dynamic range of $\pm 5,000 \mu\epsilon$, and an operation temperature range from -40°C to 120°C . The second strain sensor is the OS3120 FBG sensor as shown in Figure 7(b), which is packaged by a stainless steel carrier to protect the fiber. It has the same strain sensitivity and operation temperature range as the bare FBG sensor (OS1100), but half of the dynamic range of $\pm 2,500 \mu\epsilon$. In addition, the OS3120 has a cost three times higher than the bare OS1100 FBG sensors.

The temperature sensor selected in this study is the OS4210 FBG sensor as shown in Figure 7(c), which is sealed by a stainless steel tube to protect the sensor and eliminate the strain effect. The OS4210 FBG sensor is used as a reference sensor that can compensate the thermal effect on FBG strain sensors. It has a temperature sensitivity of $10 \text{ pm}/^\circ\text{C}$ and the operating temperature range from -200°C to 275°C .

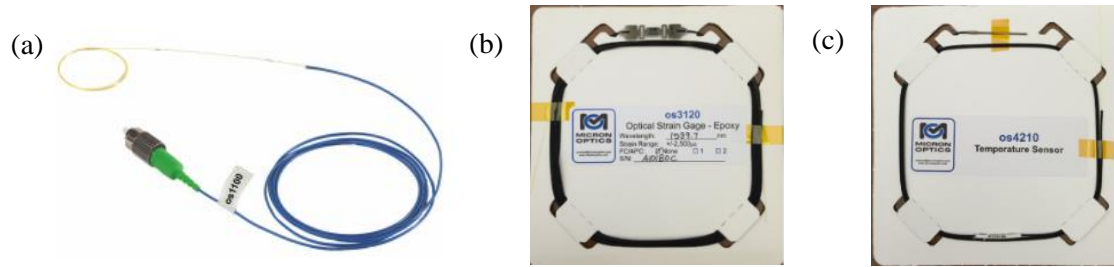


Figure 7. (a) The OS1100 Bare FBG Sensor, (b) The OS3120 Steel Packaged Sensor, and (c) The OS4210 Temperature FBG Sensor

2.4. Sensor Calibration

Laboratory calibration tests were conducted in the Material Laboratory at the department of Civil and Environmental Engineering, NDSU, to validate the strain and temperature sensitivity of the selected FBG sensors. The OS1100 FBG strain sensor was attached on an aluminum bar together with one electrical resistant gauge for strain measurement calibration test as shown in Figure 8(a). The SATEC tensile machine as shown in Figure 8(b) had been used for the loading of the strain sensor calibration test.

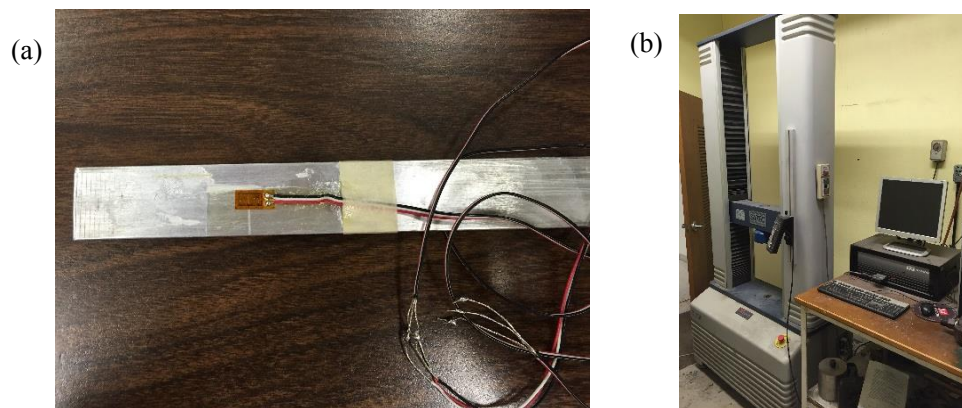


Figure 8. (a) Sample Used in Calibration Test and (b) SATEC Tensile Machine

Two calibration tests were operated with two different loading rates. The first test had a loading rate of 62.2 N/s, and a maximum load of 10 kN. The second test had a loading rate of 17.8

N/s, and the same maximum load of 10 kN. A personal computer was used to collect the strains detected by strain gauge and the wavelength changes from the FBG sensor was recorded using the NI PXIe-1017 optical spectrum analyzer. Figures 9(a, b) show the results of the two calibration tests, respectively. The obtained sensitivity of the FBG strain sensor is 1.07pm/με. Comparing the strain sensitivity provided on specification of the OS1100 FBG sensor of 1.2 pm/με, the sensor behavior is reasonable and within the tolerance range.

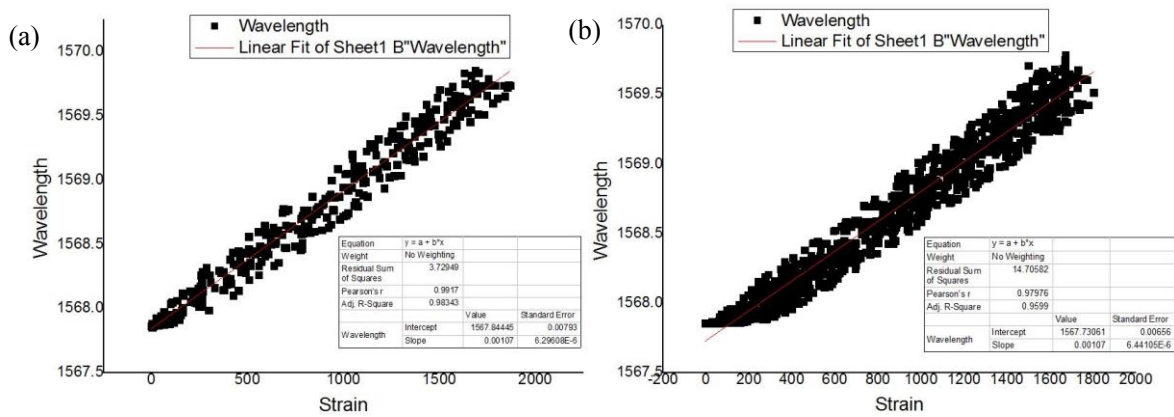


Figure 9. (a) Calibration Test Results at Loading Rate of 62.2 N/s and (b) Loading Rate of 17.8 N/s

The FBG temperature sensor was calibrated by placing the sensor into a temperature control chamber. The temperature changed from -200°C to 300°C. The FBG center wavelength changes were collected using the NI PXIe-1017 optical spectrum analyzer. Figure 9 shows the temperature calibration results. At room temperature, the OS4210 FBG temperature sensor has a temperature sensitivity of 9.5pm/ °C. It falls in the temperature sensitivity provided by manufacturer that is 10pm/ °C with a 1.7 pm/ °C tolerance, indicating a good sensor performance.

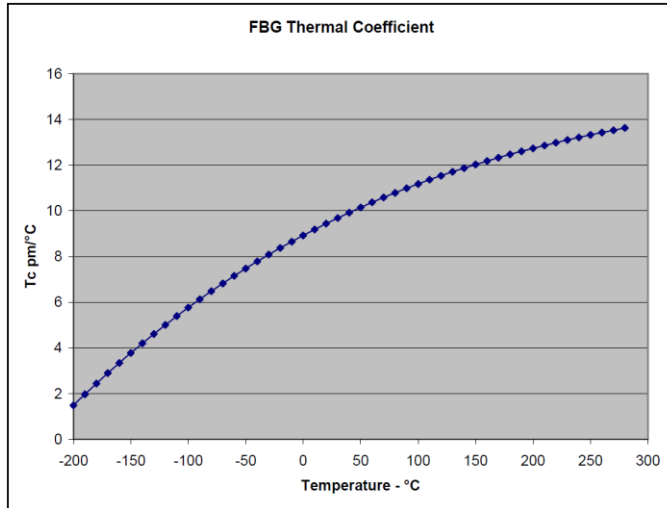


Figure 10. Temperature Calibration Test Results

2.5. Summary

In this chapter, the FBG sensors had been selected as sensing units for the in-line fiber optic sensing system for the purpose of pipeline corrosion detection. The operational principle of FBG sensor and potential corrosion detection concepts using FBG sensors were discussed in detail. Specifically, three types of sensors will be further investigated, including the bare FBG strain sensor (OS1100), the steel carrier packaged FBG strain sensor (OS3120), and the steel tube packaged FBG temperature sensor (OS4210).

Laboratory calibration tests were performed for the selected bare FBG sensor and FBG temperature sensor. The sensitivity of the FBG strain sensor is $1.07\text{pm}/\mu\epsilon$ and that for the temperature sensor is $9.5\text{pm}/^\circ\text{C}$. The sensors satisfied research requirements and the calibration results showed the sensors performed well.

3. DEVELOPMENT OF SENSOR EMBEDMENT TECHNIQUE

With FBG sensors selected for the corrosion detection purpose, in this chapter, the sensor embedment technique using thermal sprayed metallic coating is investigated. Due to the high velocity and high temperature during a thermal spraying process, the development of sensor embedment technique is one of the most challenging issues. In this study, four different embedment techniques will be tested including securing the coating using tapes, epoxy, a combination of hypodermic tube and epoxy, and a combination of hypodermic tube and high-temperature adhesives. The HVOF thermal spray coating had been done by Hard Coating Research Laboratory (HCRL) in Mechanical Engineering department of North Dakota State University.

3.1. Securing Bare FBG Sensors with Tapes During the HVOF Process

In the first trail for the FBG sensor embedment, one OS110 bare FBG strain sensor and one OS4210 FBG temperature sensor had been attached on a plate using tapes on bottom of the sensing units. The communication fibers of the FBG sensors are able to move freely without any protection. Figures 10(a, b) show the test set-up for the first trail.

The HVOF thermal spraying coating process was performed in a closed space at the Department of Mechanical Engineering, NDSU, with a self-contained air-conditioning system. A controllable robotic spraying arm with spraying gun was developed for a uniform spraying coating deposit as can be seen in Figure 11. The robotic spraying arm can automatically control the spray gun to follow the designed coating routes horizontally and vertically. The speed of the

movement and the total numbers of rounds can also be input for a specific coating requirement as well.

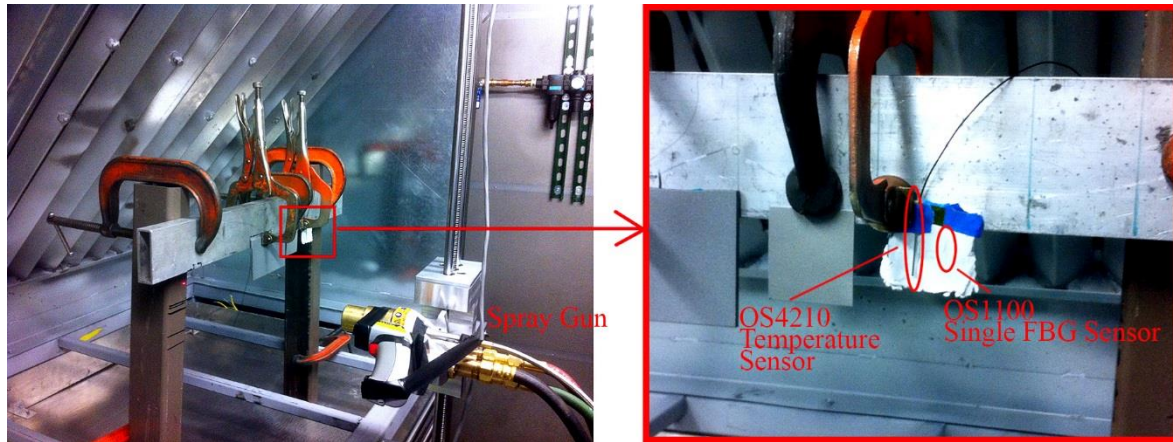


Figure 11. Thermal Spraying Robotic Arm and Test Set-up for the First Embedment Test

Figures 12(a, b) show the recorded center wavelength changes of the OS1100 FBG strain sensor and the FBG temperature sensor. Two peaks of Bragg wavelength changes were notified on each sensor and no data were obtained after that. It indicates that after two horizontal rounds of automatic spraying through the coating process, the sensors failed. From Figure 11(b), it can be seen that the maximum temperature on the surface of substrate was detected around 150°C . With an operating temperature range up to 200°C , the FBG sensors were expected to survive the heat generated during the coating process.

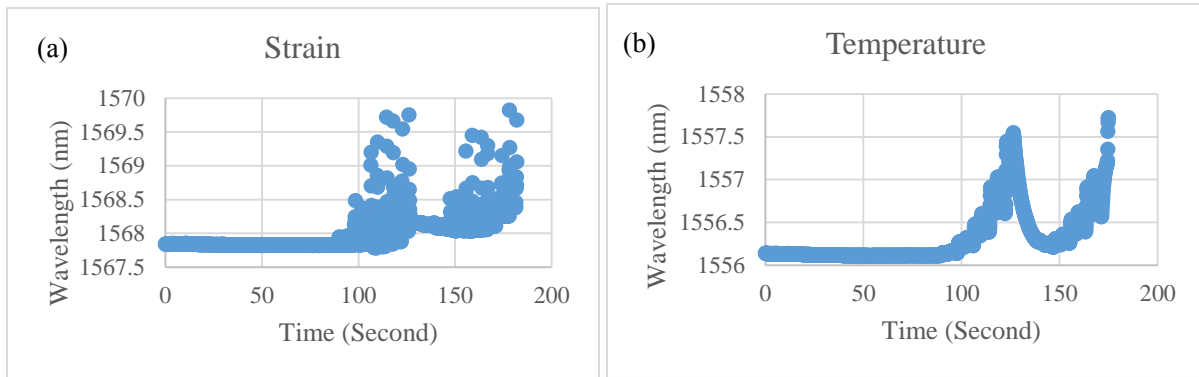


Figure 12. (a) Recorded Strain Sensor Data and (b) Temperature Sensor Data in First Test

A visual inspection was performed for the testing scene after the failure of embedment of the first trail, and it was worth noting that the fiber optic sensors were blew away during the coating process due to the high-velocity of spraying stream. Thus, the failure of the first embedment technique attributes to the deboning of the tape during the spraying process, indicating a stronger attachment technique is required for a potential successful embedment. Several points learning from the first trail for sensor embedment are summarized as below:

- (1) Exposing the bare fiber to the high-velocity spraying stream would damage the sensor;
- (2) The communication fiber for the sensor needs to be protected;
- (3) The temperature on the coating surface during the spraying process is less than the sensors' operational range and the sensors could survive the high temperature environment throughout the thermal spraying process.

3.2. Attaching FBG Sensors in Place Using Epoxy

A thin layer of epoxy was applied on the FBG sensors in the second trail to improve the bonding between the FBG sensor and the substrate and eliminate the effects from the high-velocity

spraying stream during HVOF process. One OS1100 FBG bare strain sensor, one OS3120 FBG steel carrier packaged sensor, and one OS4210 FBG temperature sensor were attached as shown in Figure 12(a). The M-Bond 200 epoxy was applied as the adhesive for the attachment, which is widely used to bond strain gauge on metal substrate. In addition, the communication fiber was protected in a flexible aluminum tube for protection as shown in Figure 13(b).

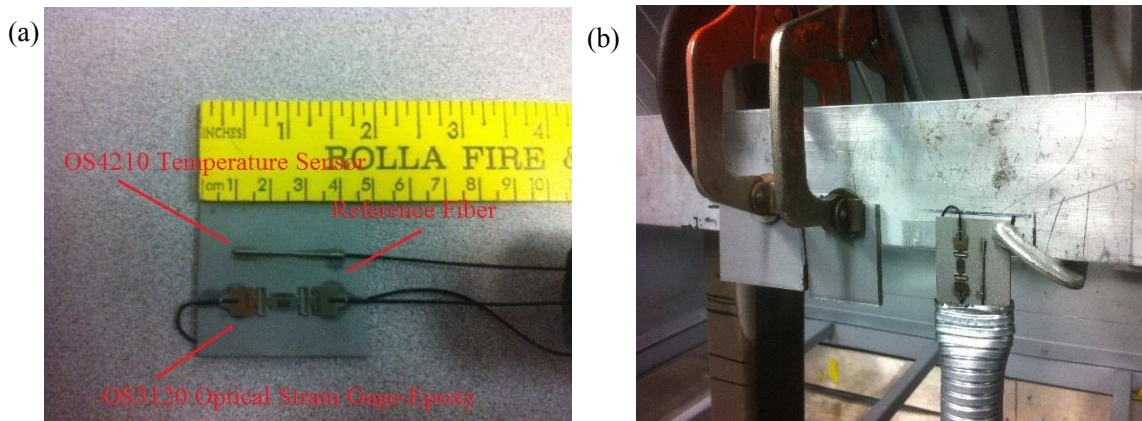


Figure 13. (a) Sensor Attached on a Steel Plate Using M-Bond 200 and (b) Sensor Embedment Test Set-up

Figures 14(a, b) show the recorded center wavelength changes of the OS31200 packaged FBG strain sensor and the FBG temperature sensor during the thermal spraying coating process. Three peaks of Bragg wavelength changes were notified on each sensor and no data were obtained after that. It indicates that after three horizontal rounds of robotic spraying arm through the coating process, the sensors failed. The reading from the FBG sensors showed a maximum coating temperature of 75°C and the maximum strain of $1,000\mu\epsilon$ throughout the three rounds of spraying coating process. With an operational temperature above 150°C and a maximum strain limit of $2,500\mu\epsilon$, the FBG sensors could possibly survive.

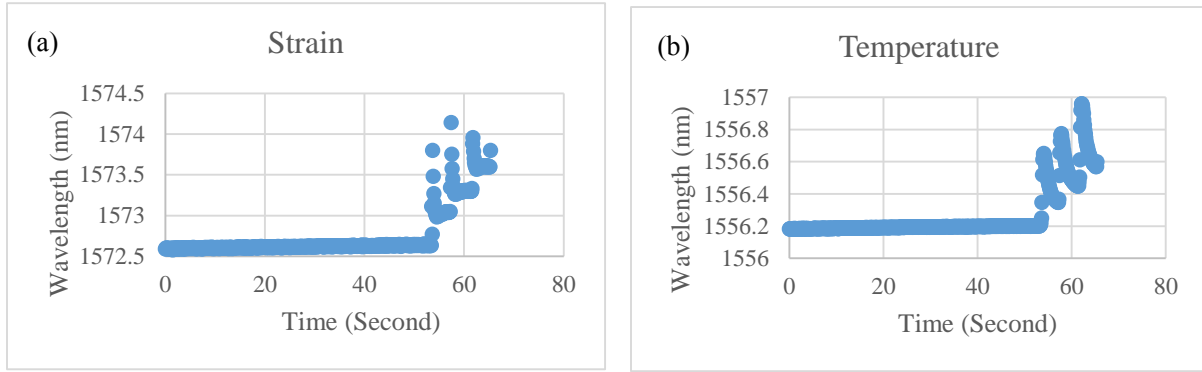


Figure 14. (a) Recorded Strain Sensor Data and (b) Temperature Sensor Data in Second Test

A visual inspection was performed for the testing sample after the failure of the second embedment test as seen in Figure 15. It is found that the bare fiber OS1100 FBG strain sensor was totally damaged by the spraying process and the steel carrier packaged OS3120 FBG sensor failed because of the small unprotected portion along the sensor was damaged by the high-velocity spraying stream. The OS4210 FBG temperature sensor was still in a good condition, however, no coating was bonded on the sensor. The absence of the coating may attribute to the smooth surface of the steel tube of the OS4210 sensor without sandblasting and the uneven surface with the substrate.

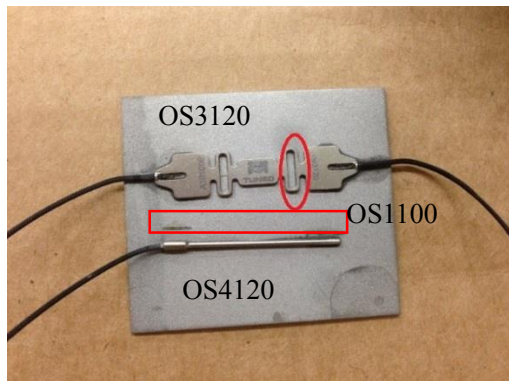


Figure 15. Damaged Area of the OS3120 FBG Sensor after the Second Trail

The findings from the second trail of the FBG embedment testing through HVOF process can be summarized as follow:

- (1) The M-Bond 200 epoxy is able to attach and keep the FBG sensors on the substrate, but not strong enough to protect the bare fiber from damage with a high-velocity spraying stream;
- (2) The OS3120 steel carrier packaged FBG sensor is not a good choice of strain sensor for embedment inside the HVOE sprayed hard coating due to the existing of a small unprotected portion on the sensor;
- (3) The HVOF sprayed coating is not able to be bonded on the surface of the OS4210 temperature sensor;
- (4) The flexible aluminum tube can protect the communication cables and fibers from influencing by the high-velocity stream.

3.3. Protecting Sensors by A Combination of Hypodermic Tube and Epoxy

The OS3120 sensor was not used in the following tests due to the poor embedment performance of the OS3120 FBG strain sensor during the HVOF spraying process and the high cost associated with this sensor. New approaches of protecting the bare fiber OS1100 FBG strain sensor against the damages from the high-velocity spraying stream during the HVOF process continued to being investigated.

In the third trail, a hypodermic tube with an inner diameter of 0.01225 inches was used to package the OS1100 FBG strain sensor. The FBG strain sensor was bonded to the hypodermic tube at both ends for strain measurements. Two semicircle grooves with a diameter of 0.4 inches

were prefabricated on the substrate to have an even surface between the embedded sensor and the substrate, as shown in Figure 16(a). The hypodermic tube packaged OS1100 FBG strain sensor can be fully embedded inside the groove and half of the OS4210 FBG temperature sensor can be embedded inside the groove. The M-Bond 200 epoxy was applied on FBG sensors for the attachment purpose.

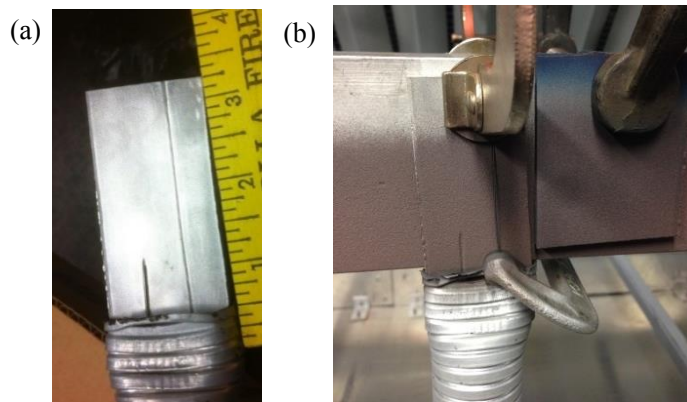


Figure 16. (a) Prefabricated Grooves on the Substrate and (b) Sensor Condition after Coating

Figure 16(b) shows the sensor condition after 10 rounds of HVOF thermal spraying. Both FBG sensors showed positive trends for survival after the entire spray coating process. However, no coating was bonded on both sensors. The absence of the coating may attribute to the smooth surface of the tubes. In addition, with temperature rising significantly during the coating process, direct exposure of the hypodermic tube to the generated heat during the coating process induced significant buckling on the longitudinal direction of the tube. The strain sensor with limited dynamic range is not able to withstand such a numerous deformation and induced damage to the strain sensor. The findings from the third trail are summarized as below:

- (1) The M-bond 200 is not sufficient to provide a rough surface for the thermal spraying coating purpose, resulting in no coatings on both of the sensors after coating process;
- (2) The hypodermic tube packaging is good approach to protect the bare FBG sensor against the high-velocity spraying stream;
- (3) The hypodermic tube, however, if directly contact with the heat generated through the coating process, would induce significant deformation on the tube and stretch the strain sensor out of limit.

3.4. Securing Embedment Using High-Temperature Resistant Adhesives

For a rough surface to coat better and a good protection of hypodermic tube away from direct heat contact, in the fourth trail, three types of high-temperature adhesives were investigated as attachment alternatives. They include: 1) epoxy based high-temperature adhesive (Minco epoxy), 2) metallic nickel based adhesive (Durabond 920), and 3) metallic stainless steel based adhesive (Durabond 954). All of the three adhesives are able to resist temperature up to 1,100°F. The purpose of this trail is to test the feasibility of using those adhesives to attach hypodermic tube or bare optic fibers for the high-temperature and high velocity thermal spray coating process. Thus, no actual FBG sensors but bare fibers were applied in this trail.

One sample with each adhesive group was prepared for this trail as seen in Figures 17(a~c). Each sample had one bare optic fiber and one hypodermic tube attached. To have a rough surface for coating purpose, sandblasting process were applied to all the three samples. Figures 18(a~c) shows the samples after sandblasting. Figure 18(b) indicated that the nickel based adhesive failed during the sandblasting process due to its brittle nature. Thus, the nickel based adhesive was

eliminated for further testing. The two samples with Minco epoxy and stainless steel based adhesive were put forward for HVOF thermal spraying coating process using copper as a coating material.

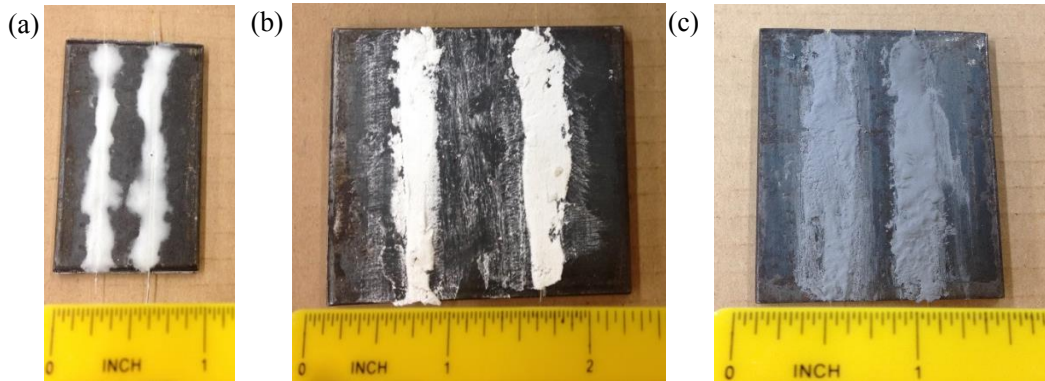


Figure 17. Samples with (a) Minco Epoxy, (b) Nickel Based Adhesive, and (c) Stainless-Steel Based Adhesive

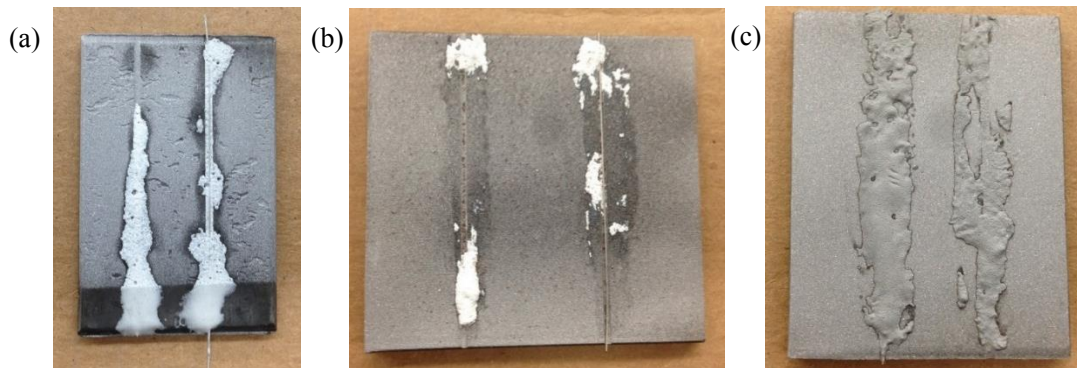


Figure 18. Samples with (a) Minco Epoxy, (b) Nickel Based Adhesive, (c) Stainless-Steel Based Adhesive after Sandblasting

Figures 19(a, b) show the two samples after the HVOF thermal spray coating process. It can be seen from Figure 19(a) that the coating failed to be bonded on the Minco Epoxy after the spraying process. The hypodermic tube was exposed after the spraying process. On the other hand, the thermal sprayed copper coating was successfully bonded on sample with the metallic-stainless steel based adhesive as can be seen from Figure 19(b). A uniform coating of $800\ \mu\text{m}$ was

successfully deposited on the metallic-stainless steel based adhesive as shown in Figure 19(c) for the optical micrograph of the cross section of the coating.

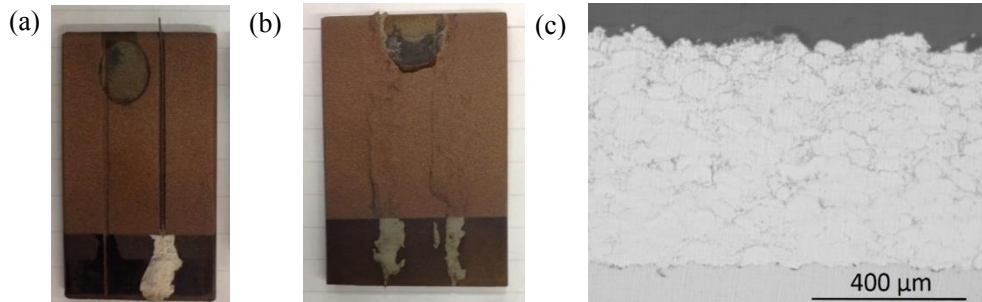


Figure 19. Samples with (a) Minco Epoxy, (b) Stainless-Steel Based Adhesive after Thermal Spray Coating process, and (c) Optical Micrograph of the Copper Coating

Several findings from the fourth trial for embedment testing are summarized as:

- (1) The Nickel Based Adhesive cannot survive the sandblasting process due to the brittle nature of the material;
- (2) The Minco high temperature epoxy is able to survive the sandblasting but fails to bond the coatings on the surface;
- (3) The Stainless-Steel Based Adhesive survives both sandblasting and coating process, and it is the best selection to protect the sensors and at the same time have a uniform metallic coating bonded on top.

3.5. Sample Preparation for Corrosion Tests

Based on the successful embedment technique identified in last section by using Stainless-Steel Based Adhesive, in this section, six samples were prepared for HVOF thermal spraying coating and further accelerated corrosion tests. The samples were using steel plates with a thickness of $\frac{1}{4}$ inches, a width of 8 inches, and a length of 3 inches, as shown in Figure 20(a). Four

of them had FBG sensors embedded among the six samples and the rest two were coating quality reference samples. Three of the samples with embedded sensors were designed to have one OS1100 FBG strain sensor on each sample and the other sample had both OS1100 FBG strain sensor and OS4210 FBG temperature sensor. As seen in Figure 20(b), the Sample #1 to Sample #3 had OS1100 sensor and Sample #4 contained both strain and temperature sensors. The Sample #5 and #6 were the reference samples for coating quality control purpose.

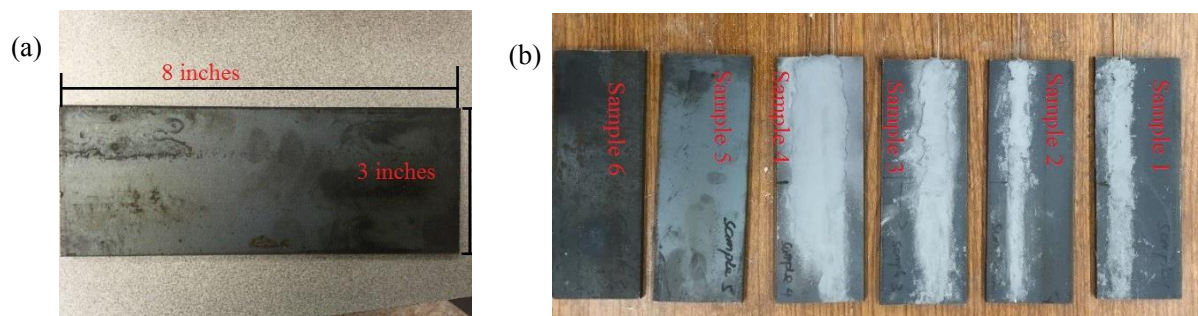


Figure 20. (a) Steel Plate Sample and (b) 6 Samples for Testing

The hypodermic tubes were used to protect the FBG sensing units as investigated in Section 3.4. A different size of hypodermic tubes had been applied at the end of the sensing unit area to protect the communication fiber at the end of the samples. The second hypodermic tube has an inner diameter of 0.028 inches, an outer diameter of 0.0425 inches, and a nominal wall thickness of 0.008 inches.

All the hypodermic tubes had been attached to the substrates using the Stainless-Steel Based Adhesive, which was approved to be successful surviving the thermal spraying process in Section 3.4. Figures 21 (a~d) show the sensor location on each samples. On Sample #4, the temperature sensor was parallel with strain sensor.

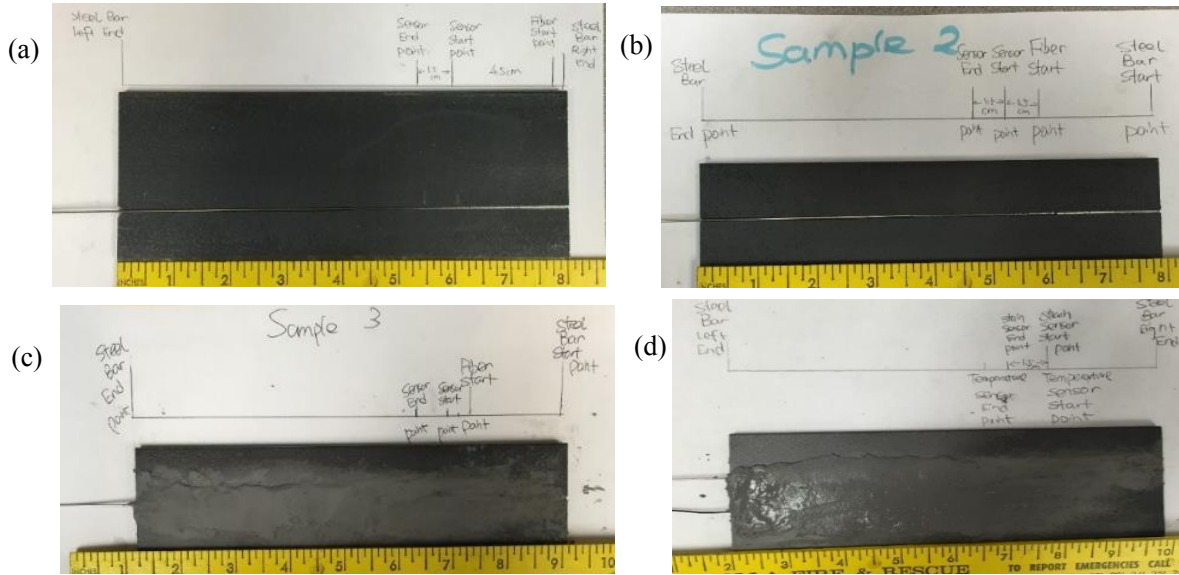


Figure 21. Sensor Location of Sample (a) #1, (b) #2, (c) #3, and (d) # 4

A 24-hour curing period was used for the Stainless-Steel Based Adhesive. Sandblasting were performed on all the samples as shown in Figure 22. The HVOF thermal spraying coating embedment was followed after sandblasting. The Aluminum Bronze Alloy (Al-Bronze, Sulzer Diamalloy 1004) Powder had been selected as the coating material in this test. It has a particle size of $45\mu\text{m}$ with a tolerance of $15\mu\text{m}$. Six thermal spraying rounds were performed using the robotic spraying arm for the coating process.



Figure 22. Sandblasted Samples

The wavelength changes of all the FBG sensors embedded in the samples along the thermal spraying coating process were collected using the NI PXIe-1071 optic spectrum analyzer continuously. Figures 23 (a~d) show the recorded FBG sensor center wavelength changes for Sample #2~#4 during the coating process. All the sensors successfully survived the thermal spraying coating process as seen in Figure 23 for the samples after coating. Six coating rounds were clearly demonstrated in all the sensor readings. With the temperature increases during the coating, all the sensors performed similarly with temperature changes. They are reasonable for this thermal spray coating process.

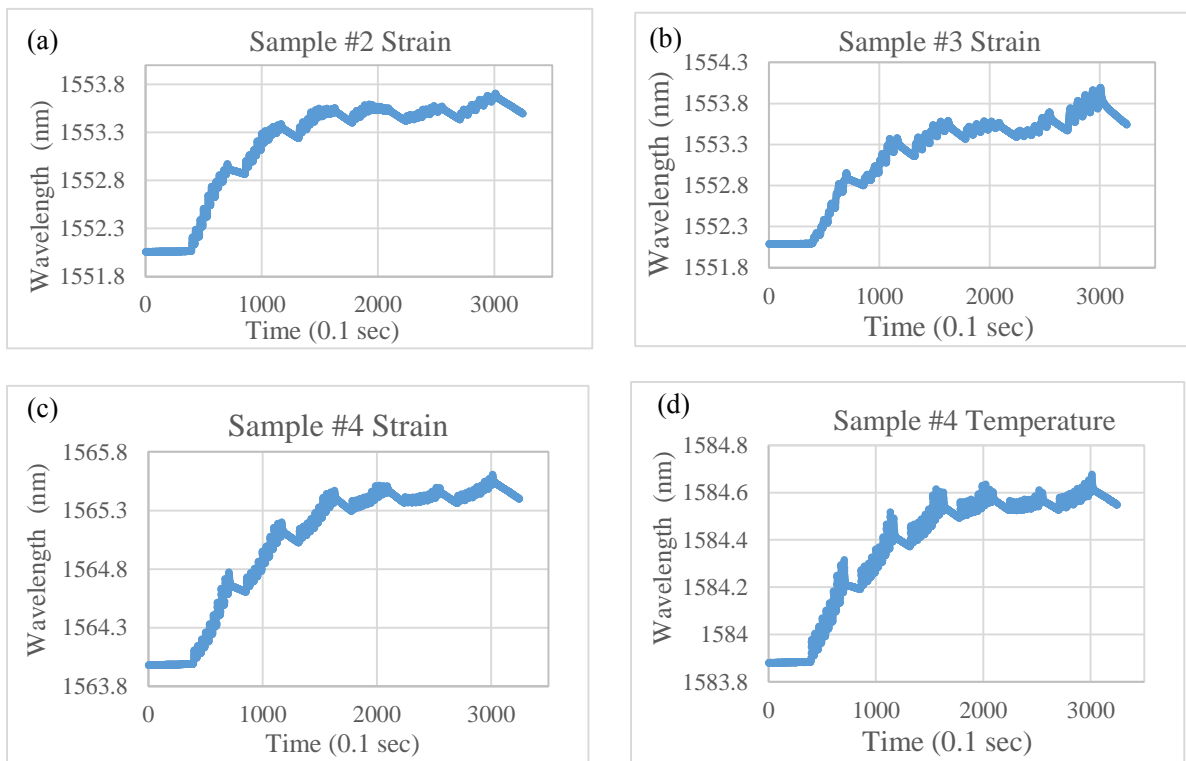


Figure 23. FBG Center Wavelength Changes during Coating Process for Sample (a) #2, (b) #3, (c) #4 Strain, (d) #4 Temperature



Figure 24. Thermal Spraying Coated Samples

Table 1 compared the FBG sensors' center wavelength changes before and after the thermal spraying coating process and the coating totally cooled down. An average center wavelength change of 1.425nm was observed during the coating process for the fiber optic strain sensors and a center wavelength change of 0.663nm was observed for the temperature fiber optic sensor.

Table 1. Center Wavelength Changes of FBG Sensors before and after Coating Process

Sample Number	Center Wavelength before Coating (nm)	Center Wavelength after Coating (nm)	Center Wavelength after Cooling (nm)
#2 Strain	1552.064	1553.496	1551.812
#3 Strain	1552.109	1553.544	1551.665
#4 Strain	1564.002	1565.402	1563.874
#4 Temperature	1583.887	1584.550	1583.827

From calibration test in Chapter 3, the bare FBG strain sensor (OS1100) has a sensitivity of 1.07 pm/ $\mu\epsilon$ and the temperature sensor (OS4120) has a sensitivity of 9.5 pm/ $^{\circ}\text{C}$. Table 2 shows the corresponding strain and temperature changes obtained from the FBG sensors during and after the coating process. An average of thermal strain of 1,329 $\mu\epsilon$ and a temperature increase of 70 $^{\circ}\text{C}$ was introduced inside the coating by the heat.

Table 2. Sensors Wavelength Analysis

Sample Number	Strain/Temperature Change after Coating ($\mu\epsilon$; $^{\circ}\text{C}$)	Strain or Temperature Change after Cooling ($\mu\epsilon$; $^{\circ}\text{C}$)	Residual Strain Change after Temperature Compensation
#2 Strain	1,338 $\mu\epsilon$	-235.5 $\mu\epsilon$	-179.4 $\mu\epsilon$
#3 Strain	1,341 $\mu\epsilon$	-415.0 $\mu\epsilon$	-331.0 $\mu\epsilon$
#4 Strain	1,308 $\mu\epsilon$	-119.6 $\mu\epsilon$	-66.5 $\mu\epsilon$
#4 Temperature	69.8 $^{\circ}\text{C}$	-6.3 $^{\circ}\text{C}$	-

The coating surface temperature that measured during coating process is around 150 $^{\circ}\text{C}$. It is different between the temperature tested during the coating process and the sensor collected temperature, which due to the temperature had been collected by sensor was reduced by high-temperature resistant adhesive. The environmental temperature drops 6.3 $^{\circ}\text{C}$ when compared to that before the coating after coating cooling down. The coating had a thermal residual strain of an average of 192 $\mu\epsilon$ in compression with the entire processes considered.

3.6. Summary

In this chapter, the sensor embedment technique had been developed successfully. Four trails were tested including securing the coating using tapes, epoxy, a combination of hypodermic tube and epoxy, and a combination of hypodermic tube and high-temperature adhesives. The first three trails were failed due to the high-velocity spraying stream during the HVOF process. For the last trail, three different high-temperature adhesives were applied including the epoxy based high-temperature adhesive (Minco epoxy), the metallic nickel based adhesive (Durabond 920), and the metallic stainless steel based adhesive (Durabond 954). The first two adhesives failed the coating process as well, leaving the metallic stainless steel based adhesive as the successful technique for the FBG embedment inside the HVOF sprayed hard coating in this study.

A successful way to embed the FBG sensors is to use a combination of hypodermic tube as packaging method and the stainless steel based adhesive as attachment based on all the detail investigations performed. With the successful development of the embedment technique of the FBG sensors inside the thermal sprayed coatings, six samples were prepared for further corrosion performance evaluation including four samples with embedded sensor systems. The center wavelength indicated that an average of thermal strain of 1,329 $\mu\epsilon$ and a temperature increase of 70 °C was introduced inside the coating by the heat during the coating process. The coating had a thermal residual strain of an average of 192 $\mu\epsilon$ in compression after cooling.

4. ACCELERATED CORROSION TESTS

With the samples prepared in Chapter 4, in this chapter, accelerated corrosion tests were performed on these samples using two different corrosion detection methods: the traditional electrochemical method and the developed in-line fiber optic sensing system, in the Mechanical Engineering laboratory at NDSU. The fundamental theory for the electrochemical method, the corrosion rate measured using the electrochemical method, and corrosion status measured by the developed in-line fiber optic sensing system are introduced in detail in this chapter.

4.1. Fundamentals of Electrochemical Corrosion Testing Method

Electrochemical accelerated corrosion test as shown in Figure 25 generally is used to test the corrosion rate of the material in a short time period. The corrosion rate is determined by the equilibrium between opposing electrochemical reactions as described in Equations (1~2). One is the anodic reaction which releases electrons into metal and is oxidized. Another one is cathodic reaction which absorbs electrons from metal. Since the two reactions are in state of equilibrium, there is no electrical current flow occurs. The equilibrium potential assumed by the metal in the absence of electrical connections to the metal is called open circuit potential. It is the primary data should be detected in most of electrochemical corrosion test [55]. A stable open circuit potential reflect as a steady state of electrons exchange. Under the steady state, the corrosion reaction rate could be assumed as a constant. The value of either the anodic or cathodic current at open circuit potential generally is known called corrosion current, which is a critical characteristic to measure the corrosion rate.

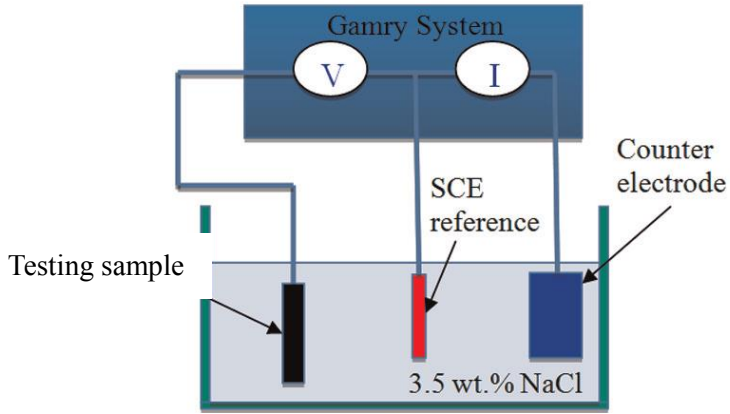


Figure 25. Electrochemical Reaction Principle

Instead of measuring the corrosion current, the estimation relation between current and potential can also be used to measure the corrosion rate, which is known as the Tafel test. The corrosion current can be calculate based on the measured potential using the Tafel equation [66]:

$$I = I_0 e^{(2.3(E-E^{\circ})/\beta)} \quad (7)$$

where, the I_0 is exchange current, E is the electrode potential, E° is the equilibrium potential, and β is the reaction's Tafel constant with the unit of volts/decade.

To describe both the anodic and cathodic reactions, the Butler-Volmer equation [66] is used:

$$I = I_a + I_c = I_{corr} (e^{(2.3(E-E_{oc})/\beta_a)} - e^{(-2.3(E-E_{oc})/\beta_c)}) \quad (8)$$

where, E_{oc} is the corrosion potential in volts, β_a is the anodic Tafel constant, and β_c is cathodic Tafel constant.

In case the potential is close to corrosion potential, the current changes linearly with the voltage approximately. The slope of the linear relation called polarization resistance. Thus, the Butler-Volmer equation can be simplified as the Stern-Geary equation [66]:

$$I_{corr} = \frac{\beta_a \beta_c}{2.3R_p (\beta_a + \beta_c)} \quad (9)$$

where, the R_p is the polarization resistance.

Thus, based on the Faraday's Law, the corrosion rate of the object can be calculated as [66]:

$$CR = \frac{I_{corr} K EW}{dA} \quad (10)$$

in which, CR represents corrosion rate with unit mm per year or milli-inches per year, K is a constant defines corrosion rate, EW is the equivalent weight of object, d is the density of testing material, and A is the testing area.

4.2. Laboratory Electrochemical Corrosion Tests and Results

In this study, a Gamry Reference 600 Potentiostat/Galvanostat/ZRA instrument, as shown in Figure 26, had been used to analyze the corrosion performance of the coated samples prepared in last chapter.



Figure 26. Accelerated Corrosion Test Set-up

The electrochemical accelerated corrosion test is performed by submerging the test samples in 3.5% NaCl solution as shown in Figure 24. In this study, to secure the 3.5% NaCl solution on the surface of coated samples, a PVC pipe was glued on top of each sample's coated surface. Loctite epoxy had been used to attach the pipe on the surface of the samples. The diameter of PVC pipe was 40.39 mm as shown in Figures 27. A 24-hour curing time in room temperature was used to allow the epoxy reaching its maximum strength.

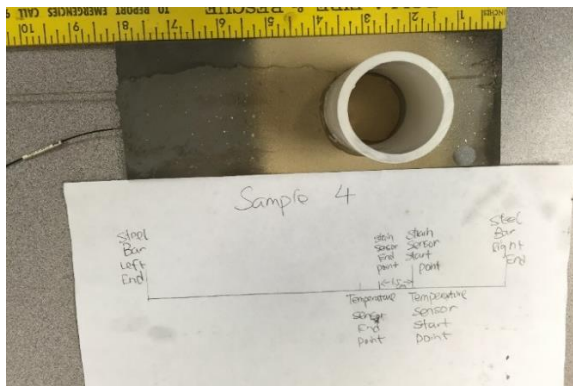


Figure 27. Glued Tube on the Sample Surface

With the samples prepared, 3.5% NaCl solution was added into the PVC pipes for electrochemical accelerated corrosion tests in an enclosed space. Six leads including two leads for electrodes, as seen in Figure 28(a), need to connect with the measurement equipment in a correct manner as shown in Figure 28(b) to perform the corrosion measurements. After connecting all leads to the sample, the polarization resistance test and open circuit potential test were performed. The equivalent weight of this coating material is 29.44 gram/equivalent, and the density is 4.1 gram/cm³. The area of the corrosion test had been performed which is the cross section area of

PVC pipe is 51.22 cm². The sample area, density, and equivalent weight were input into the instrument. All the test procedures followed the standard of ASTM G59 manual.

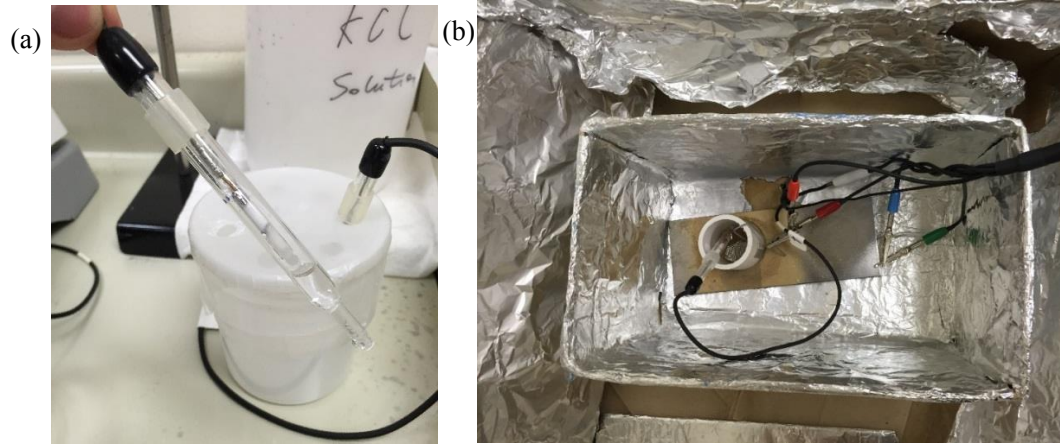


Figure 28. (a) Reference Electrode and (b) Accelerated Corrosion Test Set-up

The four coated samples with embedded sensors were tested using the procedures described above. With the polarization resistance, the Tafel tests were performed. Figures 29 (a~d) show the voltage (Y) change versus log-scale current (X) change for all the samples, respectively. The Tafel region contains the critical data, and the β_a and β_c will be calculated based on the data in the Tafel region.

Based on Figure 28, the β_a , β_c , and CR in Equation 5 and 10 had been calculated for all samples (generally the β_a varies from 0.06 to 0.12 V/decade, and the β_c varies from 0.06 to infinity) as shown in Table 3. An average corrosion rate of 0.3591 mill/year was obtained from the electrochemical method with a variance of 0.0958 mill/year. Compared to a regular carbon steel, which has a corrosion rate between 1~2 mill/year, a thin layer of thermal sprayed Al-Bronze Alloy coating material improved the corrosion resistance three times.

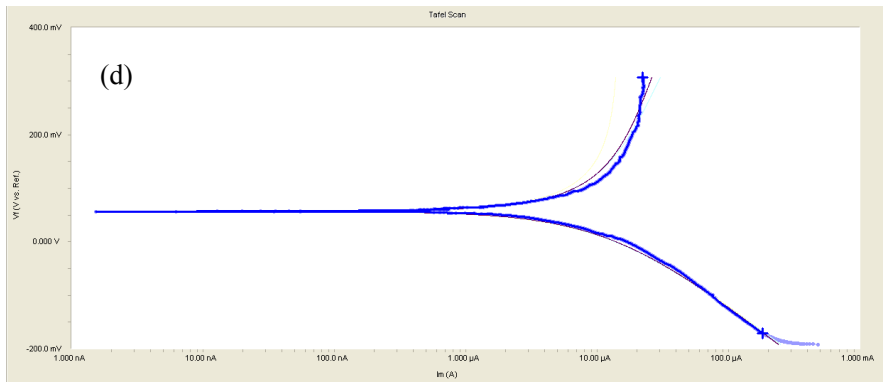
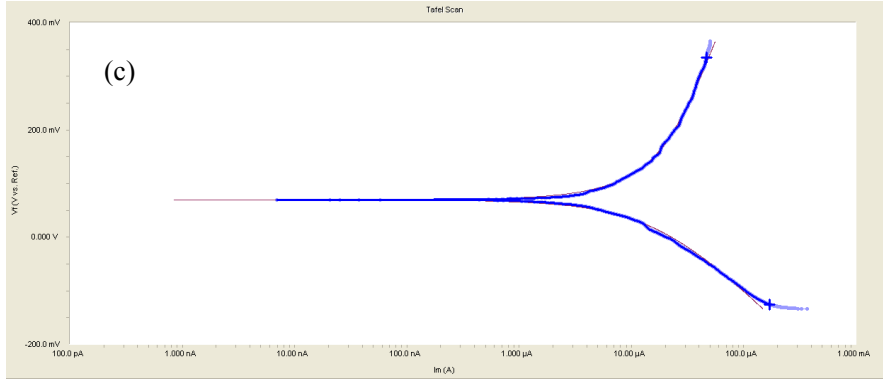
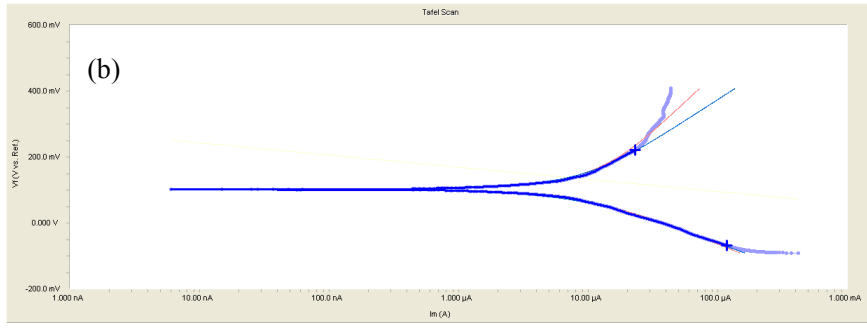
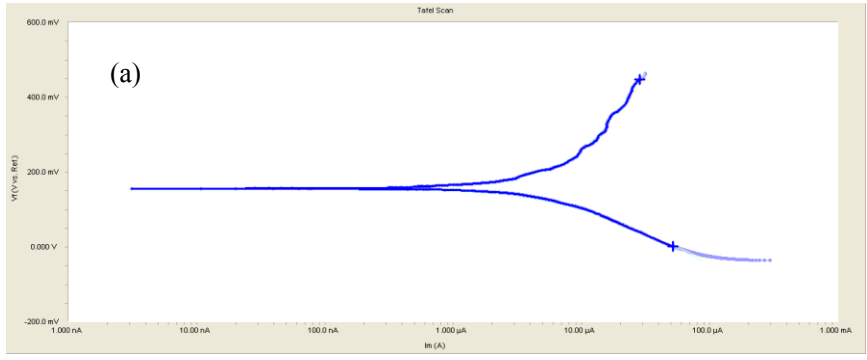


Figure 29. Tafel Test Result for Sample (a) #1, (b) #2, (c) #3, and (d) #4

Table 3. Measured Corrosion Rate for Coated Samples from Electrochemical Method

Sample Number	Anodic Tafel Constant, β_a , (V/decade)	Cathodic Tafel Constant, β_c , (V/decade)	Polarization Resistance (kohms)	Corrosion Current (amps)	Corrosion Rate (mill/year)
Sample 1	0.4424	0.1654	3.2	1.636×10^{-5}	0.2953
Sample 2	0.254	0.1499	2.9	1.413×10^{-5}	0.2552
Sample 3	0.5348	0.2047	2.3	2.798×10^{-5}	0.5054
Sample 4	0.5455	0.1806	2.8	2.107×10^{-5}	0.3803

4.3. Corrosion Detection Using The Developed In-line FBG Sensors

After the electrochemical corrosion tests, accelerated corrosion tests using the in-line FBG sensors were performed by submerging the PVC tubes with 3.5% NaCl solution for 21 days. The center wavelength changes of the four samples with embedded sensors had been recorded continuously for these 21 days with a sampling frequency of 10Hz.

Figures 30 (a~d) show the photos had been taken of each sample consistently during these 21 days for visual inspection. By comparing a sample each day from the photos, it is easily to figure out for Sample #1 and #2, the corrosion area was exactly above the embedded sensors. Since Sample #3 had been corroded before corrosion test, the corrosion area was larger than other samples. Sample #4 had less corrosion occurred which may be induced by a lower concentration of NaCl solution.



Figure 30. Corrosion visual inspection for Sample (a) #1, (b) #2, (c) #3, and (d) #4



Figure 30. Corrosion visual inspection for Sample (a) #1, (b) #2, (c) #3, and (d) #4 (continued)

Figure 31 shows the obtained FBG center wavelength changes with submerging time after eliminating the temperature effect for the 21 days. All the four samples had an approximately same

trend during the 21 days of corrosion test period. Sample #3 was corroded before the 7-day test as shown in the bottom inset in Figure 30 for the sudden drops of the wavelength changes. So no further monitoring was performed on Sample #3 after 7 days. A total changes of 60pm for Sample #2 and 30pm for Sample #1 and 4 were noticed from the test results. After 15 days, consistently, all the samples were corroded into the coating as can be seen from the bottom right inset of Figure 30.

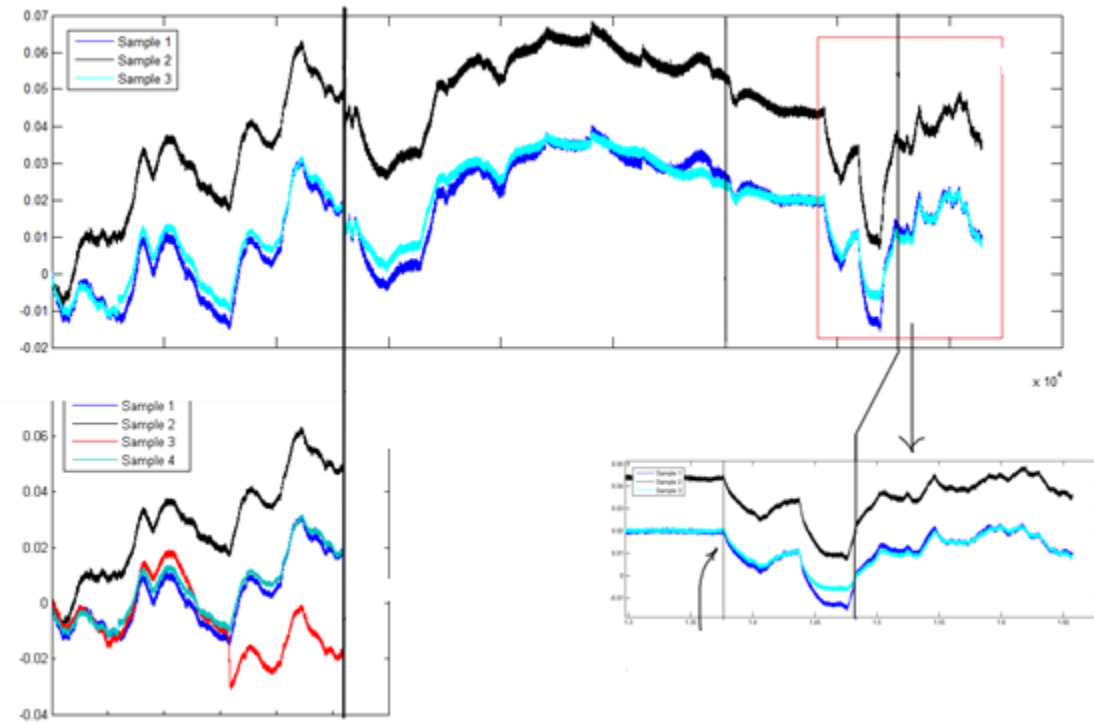


Figure 31. Center Wavelength Change from the FBG Sensors from the Accelerated Corrosion Test for 21 days

4.4. Summary

In this chapter, the laboratory accelerated corrosion tests were performed using electrochemical method. The electrochemical method indicated that an average corrosion rate of

0.3591 mill/year with a variance of 0.0958 mill/year. Compared to a regular carbon steel with a corrosion rate between 1~2 mill/year, a thin layer of thermal sprayed Al-Bronze Alloy coating material improved the corrosion resistance.

On the other hand, laboratory accelerated corrosion tests were performed on the four coated samples using the developed in-line fiber optic sensing system by submerging the coated samples in 3.5% NaCl solution for 21 days. The monitored center wavelength changed in a similar manner or same trend for all the four samples with submerging time after eliminating the temperature effect for 21 days. A total center wavelength changes of 60pm for Sample #2 and 30pm for Sample #1 and 4 were noticed from the test results, which can be further correlated to the corrosion rate or extent and potentially used for pipeline corrosion measurements.

5. CONCLUSION AND FUTURE WORK

In this thesis, an innovative inline fiber optic sensing system was developed to potentially detect the corrosion form metallic pipelines. Based on the systemic study, the following conclusions can be draw:

- 1) The bare fiber Bragg grating sensor embedded inside metallic hard coating using HVOF thermal spraying coating process was selected for the purpose of physical based corrosion detection;
- 2) Challenges to embed the FBG sensors inside the HVOF thermal spraying coatings were noticed and solved by using a combination of hypodermic tube packaged FBG sensor and stainless-steel based adhesive as attachment. The solution was achieved by investigating four different embedment techniques including securing the coating using tapes, epoxy, a combination of hypodermic tube and epoxy, and a combination of hypodermic tube and various high-temperature adhesives;
- 3) Using the successful embedment technique, four thermal sprayed Al-Brone coated samples with embedded sensors were prepared for laboratory accelerated corrosion tests;
- 4) The electrochemical method was used to evaluate the corrosion performance of the thermal sprayed Al-Brone coating with an average corrosion rate of 0.3591 mill/year with a variance of 0.0958 mill/year, indicating an improvement of corrosion resistance compared to regular carbon steel;

5) The corrosion performance of the thermal sprayed Al-Brone coating was also monitored by the developed in-line fiber optic sensing system. The monitored center wavelength of all the four samples had the same trend of changes and an average FBG center wavelength changes of 45pm were noticed from the test results. The test results showed a notable and consistent FBG center wavelength changes, indicating a potential corrosion correlation which can be used for pipeline corrosion detection.

In future, theoretic and numerical correlations between the FBG center wavelength changes and the corrosion rate will be further investigated for a better understanding of the sensor principle. As the performed laboratory tests satisfies the preliminary expectation, more future efforts will be performed on the corrosion detections on steel pipes in laboratory and then in fields. Upon validation, the developed inline fiber optic sensing system in this study could serve as a candidate to detect, monitor, and assess the pipeline corrosion remotely, nondestructively, and in a real-time manner.

6. REFERENCES

- [1] NAICS 23712, "Oil and Gas Pipeline Construction in the US: Market Research Report." IBISWorld. 2012.
- [2] C.E. Smith, "US pipeline operators sink revenue growth into expansion." Gas and Oil Journal. 2013.
- [3] R. Tubb, "2012 Worldwide Pipeline Construction Report." Pipeline and Gas Journal. 239(1), (2012)
- [4] M. Baker, N. Jaffrezic-Renault. "Elaboration of an optical fiber corrosion sensor for aircraft application." Sensor and Actuators B: Chemical. 100, 1-8, (2004)
- [5] 6th Report of European Gas Pipeline Incident Data Group, 1970-2004, December 2005 Doc. Number EGIG 05.R.0002.
- [6] M. Lecchi, "Evaluation of predictive assessment reliability on corroded transmission pipeline." Journal of Natural Gas Science and Engineering. 3, 633-641, (2011)
- [7] S. Matthews, B. James. "Review of thermal spray coating applications in the steel industry: Part 1-Hardware in steel making to the continuous annealing process." Journal of Thermal Spray Technology. 19, 1267-1276, (2010)
- [8] G. H. Koch, M. P. H. Brongers, N. G. Thompson, Y. P. Virmani, J. H. Payer. "Corrosion costs and preventive strategies in the United States." Final report to US DOT FHWA, No. FHWA-RD-01-156, (2004)

- [9] G2MT Labs, “Cost of corrosion to exceed \$1 trillion in the United States in 2012-G2MT Labs-The future of material condition assessment.”
<http://www.g2mtlabs.com/2011/06/nace-cost-of-corrosion-study-update/>.
- [10] T. Breton, J.C. Sanchez-Gheno, J.L. Alamilia, J. Alvarez-Ramirez, “Identification of failure type in corroded pipelines: A Bayesian probabilistic approach.” *Journal of Hazardous Materials*. 179, 628-634, (2010)
- [11] C. I. Ossai, “Advances in asset management techniques: an overview of corrosion mechanisms and mitigation strategies for oil and gas pipeline.” *International Scholarly Research Network*. 2012, Article ID 570143, 10 pages (2012).
- [12] C. F. Dong, H. B. Xue, X. G. Li, H. B. Qi, and Y. F. Cheng, “Electrochemical corrosion behavior of hot-rolled steel under oxide scale in chloride solution.” *Electrochimica Acta*. 54, 4223-4228, (2009)
- [13] A. Cosham, P. Hopkins, K.A. Macdonald, “Best practice for the assessment of defects in pipelines- Corrosion.” *Engineering Failure Analysis* 14, 1245-1265, (2007).
- [14] H. A. Kishawy, H. A. Gabbar, “Review of pipeline integrity management practices.” *International Journal of Pressure Vessels and Piping* 87, 373-380, (2010).
- [15] D. N. Veritas (DNV RPG 101), “Risk based inspection of topsides static mechanical equipment”, (2001).
- [16] E. J. Carl, A. B. John, and G. T. Neil, “Improving plant reliability through corrosion monitoring.” *Scientific Surveys* 49, 3-12, (2002).

- [17] D. R. Holmes and D. B. Meadowcroft, "Physical methods in corrosion technology." *Physics in Technology* 8, 2, (1977).
- [18] C. Andrade, I. Martinez, and M. Castellote, "Feasibility of determining corrosion rates by means of stray current-induced polarization." *Journal of Applied Electrochemistry* 38, 1467-1476, (2008).
- [19] C. Andrade and C. Alonso, "Corrosion rate monitoring in the laboratory and on-site." *Construction and Building Material* 10(5), 315-328, (1996).
- [20] ASTM-G96-90. "Standard guide for online monitoring of corrosion in plant equipment (electrical and electrochemical methods)". ASTM International, (2008).
- [21] S. Papavinasam, N. S. Berke, and S. Brossia, "Advances in electrochemical techniques for corrosion monitoring and measurement." Bridgeport, ASTM International, November, (2009).
- [22] C. Andrade and C. Alonso, "On-site measurements of corrosion rate of reinforcements." *Construction and Building Materials* 15, 141-145, (2001).
- [23] V. T. Rathod, M. D. Roy, S. Gopalakrishnan. "Lamb wave based identification and parameter estimation of corrosion in metallic plate structure using a circular PWAS array." *Proceeding of the 16th SPIC Annual Symposium on Smart Structures and Materials*. 72-95, (2006).
- [24] D. G. Steven. "Sensor technology innovation for the advancement of structural health monitoring: a strategic program of US-China research for the next decade." *Smart Structures and System*. 3, 221-244, (2007).

- [25] M. R. A. Hassan, M. H. A. Bakar, K. Damnbul, and F. R. M. Adikan. "Optic-based sensors for monitoring corrosion of reinforcement rebar via an etched cladding Bragg grating." *Sensors* 12, 15820-15826, (2012).
- [26] Z. Zheng, X. Sun, Y. Lei. "Monitoring corrosion of reinforcement in concrete structures via fiber Bragg grating sensors." *Front Mechanical Engineering* 4(3), 316-319, (2009).
- [27] O. Sidek, S. Kabir, and M. H. B. Afzal, "Fiber optic-based sensing approach for corrosion detection." *Electromagnetics Research Symposium, Suzhou, China, Sept. 12-16*, (2011).
- [28] S. K. T. Grattan, P. A. M. Basheer, S. E. Taylor, W. Zhao, T. Sun, K. T. V. Grattan. "Fiber Bragg grating sensors for reinforcement corrosion monitoring in civil engineering structures." *Journal of Physics: Conference Series* 76, 12-18, (2007).
- [29] T. K. Gangopadhyay, "Prospects for fiber Bragg gratings and Fabry-Perot interferometers in fiber-optic vibration sensing." *Sensors Actuat. A: Phys* 113, 20-38, (2004).
- [30] G. Qiao, Z. Zhou, and J. Ou, "Thin Fe-C alloy solid film based fiber optic corrosion sensor." *Proc. 1st IEEE Conf. on Nano/Micro Engineered and Molecular Systems*, 541-544, (2006).
- [31] C. K. Y. Leung, K. T. Wan, and L. Chen, "A novel optical fiber sensor for steel corrosion in concrete structures." *Sensors* 8, 1960-1976, (2008).
- [32] S. Abderrahmane, A. Himour, R. Kherrat, E. Chailleux, N. Jaffrezic-Renault, and G. Stremsdoerfer, "An optical fiber corrosion sensor with an electroless deposit of Ni-P." *Sensors Actuators B* 75, 1-4, (2001).

- [33] M. Benounis and N. Jaffrezic-Renault, "Elaboration of an optical fiber corrosion sensor for aircraft applications." *Sensors Actuators B* 100, 1–8, (2004).
- [34] S. Dong, G. Peng, and Y. Luo, "Preparation techniques of metal clad fibers for corrosion monitoring of steel materials." *Smart Mater. Struct* 16, 733–738, (2007).
- [35] K. R. Cooper and L. Innovations, "Optical fiber-based corrosion sensor systems for health monitoring of aging aircraft." *Proc. IEEE* 128, 847–856, (2001).
- [36] Y. Huang, Z. Gao, Z. Zhou, G. Chen, and H. Xiao, "Long period fiber grating sensors coated with nano iron/silica particles for corrosion monitoring", *Smart Materials and Structure* 22(7), 075018, (2013).
- [37] Y. Huang, F. Tang, X. Liang, G. Chen, H. Xiao, and F. Azarmi, "Steel bar corrosion monitoring with long period fiber grating sensors coated with nano iron/silica particles and polyurethane", *Structural Health Monitoring*, November 24, 2014 1475921714560070, (2014).
- [38] Z. Zheng, X. Sun, and Y. Lei, "monitoring corrosion of reinforcement in concrete structures via fiber Bragg grating sensors." *Front. Mechanical Engineering* 4, 316–319, (2009).
- [39] W. Hua, H. Cai, M. Yang, X. Tong, C. Zhou, and W. Chen, "Fe–C-coated fibre Bragg grating sensor for steel corrosion monitoring." *Corrosion Science* 53, 1933–1938, (2011).
- [40] S. Yang, H. W. Cai, and J. X. Geng, "Advanced fiber grating corrosion sensors for structural health monitoring," *Proceeded of the second International Conference on*

Structural Health Monitoring of Intelligent Infrastructure. Shenzhen, China, 441-443,
(2006)

- [41] L. de Marchi Pintos, I. de Lourenco Junior, and Jean Carlos Cardozo da Silva.
“Encapsulated fiber Bragg grating sensor for strain and temperature measurement,”
Federal University of Technology- Parana, Pato Branco, Brazil.
- [42] A. Ferreira da Silva, A. F. Gonçalves, L. A. A. Ferreira, F. M. M. Araújo, P. M. Mendes, J.
H. Correia, “A smart skin PVC foil based on FBG sensors for monitoring strain and
temperature,” *IEEE Transactions on Industrial Electronics* 58, 2728-2735,
(2011).
- [43] X. Wu, H. Xue, H. Meng, W. Shen, W. Wang, C. Tan, X. Huang, “Simultaneous
measurement of temperature and strain by combining a fiber Bragg grating and the pigtail
fiber covered with epoxy resin,” *Review of Scientific Instruments* 82, 064904, 1-4, (2011).
- [44] A. Kerrouche, W. J. O. Boyle, T. Sun, K. T. V. Grattan, J. W. Schmidt, and B. Taljsten,
“Enhanced FBG sensor-based system performance assessment for monitoring strain along a
prestressed CFRP rod in structural monitoring.” *Sensors and Actuators A* 151, 127-132,
(2009).
- [45] A. Kerrouche, W. J. O. Boyle, Y. Gebremicheal, T. Sun, K. T. V. Grattan, B. Taljsten, and
A. Bennitz, “Field tests of fiber Bragg grating sensors incorporated into CFRP for railway
bridge strengthening condition monitoring.” *Sensors and Actuators A* 148, 68-74, (2008).

- [46] Y. Huang, X. Liang. “Innovative Fiber Optic Sensors for Pipeline Corrosion Monitoring,” America Society of Civil Engineering Pipeline 2014 Conference, Portland, Oregon, September 5th, (2014).
- [47] AWWA C203-97 and Addendum C203a-99, “Coal-Tar Protective Coating and Linings for Steel Water Pipelines – Enamel and Tape – Hot Applied.” AWWA, Denver, CO., 1997-1999.
- [48] S. W. Guan, “100% Solid Rigid Polyurethane Coatings Technology and Its Application on Pipeline Corrosion Protection,” ASCE Journal of Pipelines, 156-165, (2003).
- [49] G. Munger and L. D. Vincent, “Corrosion Prevention by Protective Coatings.” Second Edition, NACE International, Huston, TX, (1999).
- [50] AWWA C213-96, “Fusion-Bonded Epoxy Coating for the Interior and Exterior of Steel Water Pipeline.” AWWA, Denver, CO., (1996).
- [51] AWWA C222-99, “Polyurethane Coatings for the Interior and Exterior of Steel Pipelines and Fittings.” AWWA, Denver, CO., (1999)
- [52] Y. C. Huang, T. Y. Lo, C. G. Chao, and W. T. Whang, “Anti-corrosion characteristics of polyimide/h-boron nitride composite films with different polymer configurations.” Surface and Coatings Technology 260,113-117, (2014).
- [53] H. Koivuluoto and P. Vuoristo, “Structural analysis of cold-spray Nickel-based metallic and metallic-ceramic coatings.” Journal of Thermal Spray Technology 19, 975-989, (2009).

- [54] H. S. Grewal, H. Singh, Anupam Agrawal, “Microstructural and mechanical characterization of thermal sprayed nickel-alumina composite coatings.” *Surface and Coatings Technology* 216, 78-92, (2013).
- [55] J. Mostaghimi, S. Chandra, R. Ghafouri-Azar, and A. Dolatabadi, “Modeling thermal spray coating processes: a powerful tool in design and optimization.” *Surface and Coating Technology* 163-164. 1-11, (2003).
- [56] L. M. Berger, “Application of hardmetals as thermal spray coating.” *International Journal of Refractory Metals and Hard Materials* 49, 350-364, (2014).
- [57] M. Li and P. D. Christofides, “Modeling and control of high-velocity oxygen-fuel (HVOF) thermal spray: a tutorial review.” *Journal of Thermal Spray Technology* 18 (5-6), 753-768 (2009).
- [58] J. V. Kelley and R. Kilbane, “HVOF application of Nickel and Nickel alloy to Tungsten heavy alloy for jacketed penetrators.” ARL-TR-3095, U.S. Army Research Laboratory, (2003).
- [59] Y. Jiang, Y. Yan, K. Y. L. Christopher. “Optical fiber grating corrosion sensors.” *Acta Photonica Sinica* 35,96-99, (2006).
- [60] FBGS Draw Tower Gratings, “FBG-Fiber Bragg grating principle.”
<http://www.fbgs.com/technology/fbg-principle>
- [61] M. H. Maher, E. G. Nawy, “Evaluation of fiber optic Bragg grating strain sensors in high strength concrete beams.” *Applications of Fiber Optic Sensors in Engineering Mechanics*, ASCE-EMD, ASCE, New York, 120–133, (1993).

- [62] J. Bruno, A. Costa, and J. A. Figueiras, "Fiber optic based monitoring system applied to a centenary metallic arch bridge: design and installation." *Engineering structure* 44, 271-280, (2012).
- [63] J. Gao, J. Wu, J. Li, and, X. Zhao, "Monitoring of corrosion in reinforced concrete structure using Bragg grating sensing." *Nondestructive Testing and Evaluation International* 44, 202-205, (2011).
- [64] M. R. A. Hassan, M. H. A. Bakar, K. Dambul, and F. R. M. Adikan, "Optical-based sensors for monitoring corrosion of reinforcement rebar via an etched cladding Bragg grating." *Sensors* 12, 15820-15826, (2012).
- [65] J. R. Lee, C. Y. Yun, and D. J. Yoon, "A structural corrosion-monitoring sensor based on a pair of prestrained fiber Bragg gratings." *Measurement Science and Technology* 21 017002, 7pp, (2010).
- [66] Gamry Instruments, "Application note: getting started with electrochemical corrosion measurement," Gamry Instruments, Inc., Rec. 1.1 1/3/2011,